Title
INVESTIGATION OF THE NEAR-SURFACE ELECTRONIC STRUCTURE OF Cr(001)

Author
Klebanoff, L.E.

Publication Date
1984-12-01

Lawrence Berkeley Laboratory
UNIVERSITY OF CALIFORNIA

Materials & Molecular Research Division

Submitted to Physical Review B

INVESTIGATION OF THE NEAR-SURFACE ELECTRONIC STRUCTURE OF Cr(001)

L.E. Klebanoff, S.W. Robey,
G. Liu, and D.A. Shirley

December 1984

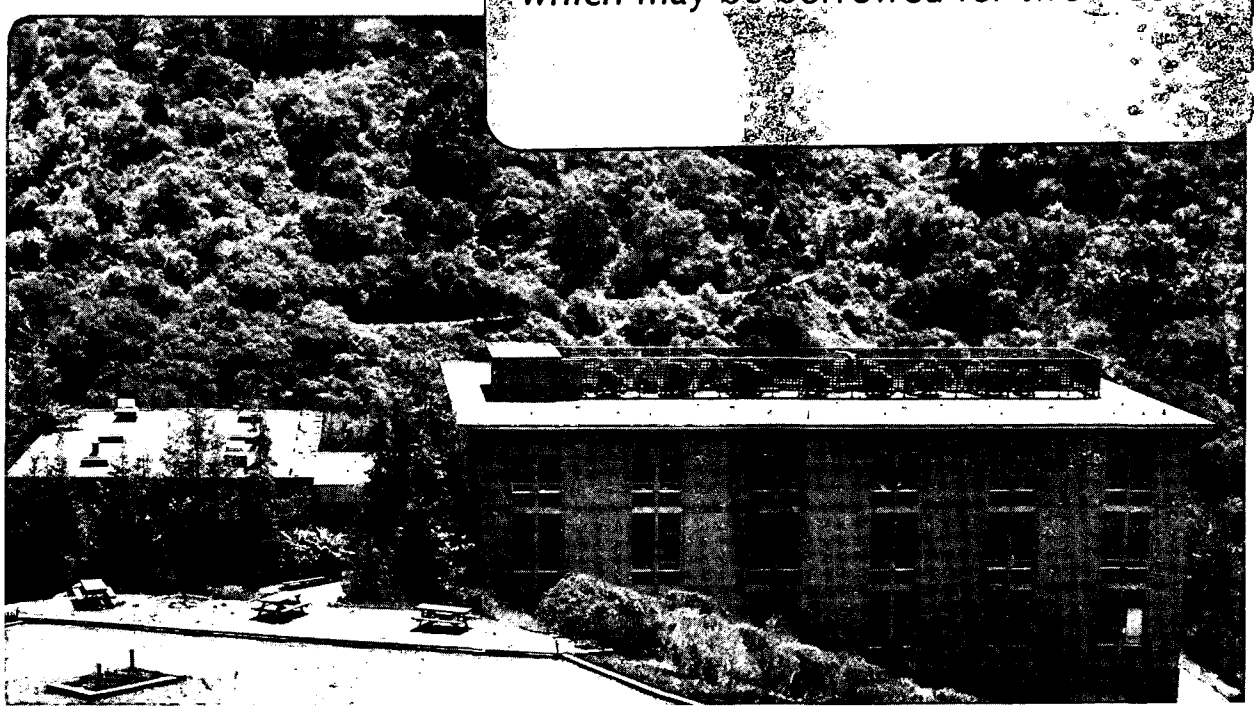

Prepared for the U.S. Department of Energy under Contract DE-AC03-76SF00098

DISCLAIMER

LBL-18633

Investigation of the Near-Surface Electronic Structure of Cr(001)

L. E. Klebanoff, S. W. Robey, G. Liu,* and D. A. Shirley

Materials and Molecular Research Division
Lawrence Berkeley Laboratory
and
Departments of Chemistry and Physics
University of California
Berkeley, California 94720

Abstract

An angle-resolved photoelectron spectroscopy (ARPES) study of Cr(001) near-surface electronic structure is presented. Measurements are reported for energy-band dispersions along the [010] direction parallel to the crystal surface. The periodicity of these band dispersions indicates that the valence electrons experience and self-consistently establish antiferromagnetism in the near-surface layers of Cr(001). We also present highly surface-sensitive ARPES measurements of the energy-band dispersions along the [001] direction normal to the surface. The results suggest that the surface magnetic moments, which couple ferromagnetically to each other within the surface layer, couple antiferromagnetically to the moments of the atoms in the second layer. Temperature-dependent studies are presented that reveal the persistence of near-surface antiferromagnetic order for temperatures up to 2.5 times the bulk Néel temperature. The temperature dependence of this antiferromagnetic order suggests that its thermal stability derives in part from the stability of the Cr(001) ferromagnetic surface phase.

*Department of Physics, Zhejiang University, Hangzhou, People's Republic of China.

I. INTRODUCTION

We report here an investigation of the near-surface electronic structure of Cr(001) using angle-resolved photoelectron spectroscopy (ARPES). The ARPES technique has itself been the subject of considerable study. To introduce the physics of the measurement that are relevant to this investigation, we will highlight the evolution of ARPES as a probe of transition metal valence electronic structure.

Over the past ten years, ARPES has developed into the most direct method for the study of the electronic structure of transition metals. Many early ARPES measurements were made on copper[1-6], for which it was easy to prepare clean unreconstructed surfaces. Copper also had the advantage of being a Pauli paramagnet. The conceptual simplicity of its paramagnetism encouraged confidence in the accuracy of existing band structure calculations.[7] The agreement between Fermi surface measurements[8] and the ab initio theoretical results suggested that the band structure for copper was understood. The result of these ARPES investigations was a qualitative understanding of valence-band photoemission.

It became clear that the ARPES technique yielded spectroscopic binding energies to which initial-state wavevectors could be assigned. Peaks in a valence-band photoemission spectrum were produced by direct (or vertical) transitions in wavevector (k) space:

$$\underset{\sim}{k}_i + \underset{\sim}{g} = \underset{\sim}{k}^f \qquad (1)$$

Here, $\underset{\sim}{k}_i$ is the wavevector (in the first Brillouin zone) of the valence-band initial state responsible for the spectral peak; $\underset{\sim}{k}^f$ is the wavevector (outside the first Brillouin zone) of the final-state photoelectron in the solid; and $\underset{\sim}{g}$ is the reciprocal lattice vector supporting the transition. The initial-state wavevector $\underset{\sim}{k}_i$ is inferred using equation (1) by the experimental determination of the final-state wavevector $\underset{\sim}{k}^f$ (to be discussed). The spectroscopic initial-state energy E_{IN} is obtained directly from the ARPES spectrum as the binding energy (referenced to the Fermi level, E_F) of the spectral peak. The interpretation of valence-band photoemission in this direct-transition model (DTM)[9] yielded initial-state $E_{IN}(\underset{\sim}{k}_i)$ values that agreed almost quantitatively with theoretical one-electron valence-band dispersion relations. Total agreement has been elusive. The remaining discrepancy between experimental and theoretical $E_{IN}(\underset{\sim}{k}_i)$ is due in part to the influence of many-body processes (screening) on the spectroscopic binding energies E_{IN} observed in the ARPES experiments.[10-12] Consistent with the DTM was the discovery that symmetry selection rules govern the photoelectric transition.[13-15] Thus, under certain experimental conditions, ARPES could determine the symmetry (group representation) of those initial states producing spectral peaks. The valence-band representation labels determined by ARPES measurements using polarized light were found to be consistent with group theory.

With these aspects of photoemission qualitatively understood, experiments were performed to investigate the effect of temperature on

the photoelectric transition. The simplicity of the paramagnetic state at elevated temperatures made the Pauli paramagnets once again the logical starting point. Measurements on copper[16] and tungsten[17,18] confirmed the theoretical prediction[19] that the thermal excitation of initial-state phonons leads to phonon-assisted nondirect transitions (NDT). These NDT degrade the k-space resolution of the spectroscopy. For the direct transition of equation (1), the realized percentage of direct transitions (%DT) depends on the energy of the transition (through $|g|$) and the temperature, T, via a Debye-Waller factor:

$$\frac{\%DT}{100} = e^{-[|g|^2\langle u(T)^2\rangle]/3} \qquad (2)$$

where $\langle u(T)^2\rangle$ is the mean-square atomic displacement at temperature T. To summarize, ARPES studies of paramagnetic metals established the technique's utility in determining valence-band dispersions and symmetries directly. However, at high-excitation energies (large $|g|$) or high temperature (large $\langle u(T)^2\rangle$) a loss of k-space resolution occurs.

This precedent work on paramagnets has provided the conceptual base that was necessary to extend the ARPES technique to magnetic elements. Numerous ARPES investigations have been made of ferromagnetic Fe[20] and Ni[21]. The results have shed considerable light on the valence electronic structure of these metals, and consequently on the origin of their itinerant ferromagnetism. By

comparison, few ARPES investigations have been made of the itinerant antiferromagnets Cr and Mn. The near-surface electronic structure of Cr(001) and its implications for magnetism is the subject of this investigation.

The nearly half-filled 3d band of Cr produces unique electronic and magnetic properties in the bulk metal. Neutron diffraction measurements on Cr[22-27] reveal the existence of a spin-density wave (SDW)[28] whose periodicity is incommensurate with the body-centered cubic (bcc) crystal lattice. The SDW requires nearest-neighbor atoms to possess antiparallel magnetic moments, μ. Its incommensurate periodicity causes the magnitude of these moments to vary sinusoidally:

$$\mu = \mu_0 \cos (\underset{\sim}{Q} \cdot \underset{\sim}{r}) \qquad (3)$$

Here, μ_0 is the maximum magnitude of μ; $\mu_0 = 0.59\mu_B$. The periodicity of the SDW is given by the wavevector $\underset{\sim}{Q}$; $\underset{\sim}{Q} = (1 \pm \delta) \cdot (2\pi/a) \langle 100 \rangle$. The value of δ indicates the deviation from commensurate periodicity. It is observed to be temperature dependent but is typically ~ 0.05 Å^{-1}.[22-27] The lattice constant, a, takes the value 2.884 Å.

The true incommensurate ($\delta \neq 0$) SDW ground state of bulk Cr is too complicated to be treated easily with band-structure theory. However, several calculations[29-32] have been made of a commensurate ($\delta = 0$) SDW state corresponding to perfect itinerant antiferromagnetism. The magnetic lattice of this commensurate antiferromagnetic (AF) state is shown in Fig. 1. The chromium atoms

are located on a bcc crystal lattice. However, the AF spin arrangement defines a simple cubic (sc) magnetic lattice. Consequently, the reciprocal space lattice is sc, and the associated AF Brillouin zone is a volume of simple cubic symmetry.[32] This differs fundamentally from the symmetry of the paramagnetic (PM) phase, for which the reciprocal space lattice is face-centered cubic. The associated PM Brillouin zone is a regular rhombic dodecahedron with twice the volume of the AF Brillouin zone. The relationship between the AF and PM Brillouin zones is shown in Fig. 2. A commensurate spin structure would render equivalent the two symmetry points in reciprocal space labelled (Γ) and (H) in the PM Brillouin zone.[32]

The existence of a magnetic lattice affects the periodicity of the valence-band dispersions. This is demonstrated in Fig. 3 for a model sinusoidal band along the [010] direction. In the absence of antiferromagnetism, the band would disperse with a periodicity consistent with the PM Brillouin zone, as shown in Fig. 3(a). A magnetic potential with commensurate wavevector $2\pi/a$ would mix PM states with wavevectors k and $k \pm 2\pi/a$. Thus the energy-band structure for a commensurate antiferromagnet arises from the translation of the PM energy bands by $2\pi/a$.[32] This is shown for our sinusoidal band along [010] in Fig. 3(b). An energy gap would appear at the X point where the bands cross. This is omitted for simplicity. The periodicity of the band dispersions in Fig. 3(b) is consistent with the sc Brillouin zone.

When using realistic PM valence bands in this "folding"

procedure, energy gaps appear near the Fermi level along the [110]ΓM and [111]ΓR lines of the sc Brillouin zone.[32] These gaps stabilize the SDW state. Nature chooses an incommensurate periodicity for the SDW because the ground-state of lowest energy results from the mixture of PM states differing in wavevector by $(1 \pm \delta)\cdot 2\pi/a$. This is attributed to the difference in size between the electron jacket around (Γ) and the octahedral hole pocket around (H) in the PM band structure.[33] The periodicity (and hence the Brillouin zone) of the band dispersions for an incommensurate SDW state may not be simply defined.[34] However a first-order estimate is obtained by translating the PM energy bands by $(1 \pm \delta)\cdot 2\pi/a$. This is shown in Fig. 3(c) for our sinusoidal energy band.

We expect from Fig. 3(b) that the energy bands of an ideal AF state would disperse symmetrically about the X point. In the absence of commensurate antiferromagnetism, energy-band dispersion need not show this periodicity. Figure 3(a) demonstrates that in a paramagnetic state, the same sinusoidal band would disperse about the (H) point, since this point corresponds to a zone boundary in the PM Brillouin zone. Figure 3 suggests that commensurate (Fig. 3(b)) or incommensurate (Fig. 3(c)) antiferromagnetism should be distinguishable from paramagnetism (Fig. 3(a)) by a measurement of the valence-band dispersions along the [001] or [010] axes of Fig. 2. However, to valence-band measurements with finite energy and wavevector resolution, commensurate and incommensurate AF order would seem indistinguishable. We will therefore refer to the dispersive

behavior shown in Fig. 3(b) as representative of our expectations for a general AF order. Since the nature of the magnetism in the Cr(001) near-surface layers is the subject of this study, we will not specify initially which of the Brillouin zones (AF or PM) drawn in Fig. 2 is in fact applicable. We will therefore temporarily adopt a dual notation in which the [010] and [001] symmetry lines are labelled $\Gamma(H)$-X-$\Gamma(\Gamma)$.

Most ARPES experiments probe within the first 10 atomic layers near a metal surface. Despite this surface sensitivity, for many metals semi-quantitative agreement exists between ARPES results and bulk valence-band theory. This suggests that in these metals, the electronic structure is already "bulklike" by the second or third layer. In contrast, there is considerable experimental[35] and theoretical[36-39] support for the existence of a ferromagnetic surface phase on clean Cr(001). The magnetic moment possessed by the (001) surface atoms ($\sim 2\mu_B$)[35] is much larger than the maximum bulk value ($0.59\mu_B$) observed in neutron diffraction.[25] The transition from surface to bulk electronic structure must encompass a finite number of near-surface layers. It is this near-surface region that is probed by our ARPES measurements.

Chromium's unusual electronic structure and chemical reactivity have made it a challenging system for study with ARPES. Johansson et al.[40] used normal-emission ARPES to study the energy bands of Cr(110) along the [110] ΓM symmetry line. Unfortunately their spectra indicate substantial surface contamination, as we shall explain. This

renders their results suspect. Gewinner et al.[41] made off-normal ARPES measurements of the Cr(001) surface in an attempt to probe the [010] Γ(H)-X-Γ(Γ) symmetry line. They found no evidence of antiferromagnetic band properties. On the contrary, their room-temperature results were compared with a bulk paramagnetic band calculation for the H-Δ-Γ symmetry line of the PM Brillouin zone.[41,42]

We felt that if antiferromagnetism exists in the near-surface layers of Cr(001), then it should have an influence on the periodicity of the Γ(H)-X-Γ(Γ) electronic structure, as postulated in Fig. 3(b). Thus, we have made a comprehensive ARPES investigation of the near-surface electronic structure of Cr(001) along the Γ(H)-X-Γ(Γ) symmetry line for both the [010] and [001] (surface normal) directions. The experimental details are given in Section II. The use of the DTM in data acquisition and interpretation is developed in Section III. We present in Section IV the results for the [010] and [001] band dispersions, complete with symmetry assignments. We also present in Section IV our results for the temperature dependence of the [010] electronic structure. In Section V we examine the implications of these results for the near-surface magnetism of Cr(001). The relationship of our work to prior ARPES investigations of chromium is described in Section VI. Finally, our main conclusions are summarized in Section VII.

II. EXPERIMENTAL

Almost all of our ARPES measurements employed synchrotron radiation from the Stanford Synchrotron Radiation Laboratory. Beam Line I-I was used for measurements requiring ultraviolet photon energies ($12 \leq h\nu \leq 25$ eV). Beam Line III-I covered the required soft x-ray range ($80 \leq h\nu \leq 150$ eV). For both beam lines, the radiation is about 98 percent polarized in the horizontal plane. The photon energy resolution for the ultraviolet photoelectron spectroscopy (UPS) studies was maintained at 0.10 eV FWHM, while the soft x-ray photoelectron spectroscopy (SXPS) photon energy resolution was kept below 0.35 eV FWHM. Polarization-dependent measurements at $h\nu = 21.22$ eV were made using a helium discharge lamp equipped with a 3-element polarizer. The plane of photon polarization could be rotated continuously 360° about the photon k vector.

The electron analyser[43] used for all measurements was of the electrostatic 180° hemispherical sector variety. The angular resolution was ± 3°. The kinetic energy resolution was fixed at 0.12 eV FWHM, providing an overall (photons and analyser) instrumental resolution of 0.15 eV FWHM and 0.40 eV FWHM for the UPS and SXPS measurements respectively. The electron analyser has the capacity for independent rotation in the horizontal and vertical planes. The experimental geometry for our synchrotron radiation UPS and SXPS measurements is shown in Fig. 4. Our sample manipulator provided crystal rotation

about the [001] crystal normal (azimuthal rotation) and about the [100] axis (polar rotation). The sample's azimuthal angle was oriented with the low-energy electron diffraction (LEED) pattern so that the (100) mirror plane (the plane defined by the [001] and [010] axes) contained the vector potential $\underset{\sim}{A}$ of the radiation. The sample's polar position was calibrated via laser alignment, and adjusted so that the $\underset{\sim}{A}$ vector made a 25.0° angle with the crystal normal, as shown in Fig. 4. Off-normal measurements were made by rotating the analyser away from the normal, and toward the $\underset{\sim}{A}$ vector in the (100) mirror plane. Experimental angles are accurate to within ± 0.5°. We label the photon-surface orientation of Fig. 4 P-polarization. For S-polarization ARPES measurements using 21.22 eV HeI_{α} radiation, the $\underset{\sim}{A}$ vector is rotated to lie along the [100] direction perpendicular to the (100) mirror plane.

Our sample was a high-purity chromium single crystal that was spark cut to within ± 0.5° of the (001) plane and mechanically polished (0.5μ diamond paste) to a mirror finish. As in a previous study[44], the sample was argon-ion bombarded ($5x10^{-5}$ Torr, 1.5kV) with high temperature (1120 K) cycling for three weeks to remove bulk nitrogen as detected by Auger electron spectroscopy (AES). The crystal then displayed a very sharp, low background 1X1 LEED pattern. No impurities were detectable by AES, or more sensitively, by ARPES. Even more sensitive high-resolution electron energy loss spectroscopy (HREELS) measurements on Cr(001) have subsequently confirmed that this cleaning procedure produces an adsorbate-free surface.[45]

After an hour exposure to the residual gases in our spectrometer (operating pressure = 2×10^{-10} Torr), the crystal surface became contaminated with carbon and oxygen via carbon monoxide (CO) decomposition. This produced faint, blurry spots in the c(2X2) regions of the LEED pattern, and an impurity (carbon and oxygen) 2p photoelectron peak at 6.7 eV binding energy in the ARPES spectrum. Flashing the crystal to 1120 K for three minutes removes ~ 95 percent of this impurity via CO desorption. This restores the low-background 1X1 LEED pattern, and removes the 6.7 eV impurity peak from the ARPES spectrum. Flashing the crystal in this way permits relatively uninterrupted study of the clean surface for four to five hours. After this time, we argon-ion sputtered the crystal at room temperature for one hour to remove accumulated impurity. We then annealed the crystal at 1120 K for five minutes to restore order to the clean surface.

The periodicity of the SDW in bulk chromium can be changed by small (~0.5 atomic percent) levels of transition metal impurities.[46,47] Consequently, after our experiments we analysed our crystal for such bulk contaminants. X-ray fluorescence measurements of the Cr(001) surface revealed no transition metal impurities to within the 0.05 atomic percent sensitivity of the method. This technique probes the crystal to a depth of ~1000 Å from the surface. To investigate the possibility of deep bulk contamination, we performed two independent spectrochemical analyses of portions of our crystal. To within the 0.005 atomic percent

sensitivity of these methods, no transition metal impurities could be found. Our ARPES results are thus characteristic of an extremely pure chromium sample.

High-temperature spectra were collected by flashing the crystal to 1120 K, turning off the heater, and taking quick ARPES scans during well-defined temperature intervals on the cooldown curve. Crystal temperatures were measured with a thermocouple-calibrated infra-red pyrometer, and are accurate to within ± 5 K.

III. SPECTROSCOPIC METHOD

As described in Section I, ARPES of valence bands involves a direct excitation in wavevector space (eqn. (1)). However, ARPES measures the energy $E(\underset{\sim}{p}^f)$ and wavevector $\underset{\sim}{p}^f$, of the plane-wave photoelectron state at the detector. Two complications prevent the direct relation of $\underset{\sim}{p}^f$ for a photoelectron spectral peak and $\underset{\sim}{k}_i$ for the initial state. First, an assumption must be made about the final-state dispersion relation $E(\underset{\sim}{k}^f)$ in the solid. The second concerns photoelectron refraction at the metal surface. The photoelectric transition takes place in the presence of the solid's attractive inner potential, V_0.[48] As the photoelectron traverses the surface, it passes into the potential-free vacuum region. The resulting refraction changes the wavevector component perpendicular to the surface of the photoelectron in the solid $k_\perp^f$ to the value $p_\perp^f$ measured in the vacuum. The value of $k_\perp^f$ must be <u>inferred</u> from $p_\perp^f$.[48]

A model has been developed[1,9,48] that addresses both of these questions. It has proven very useful in interpreting a large body of ARPES data. It is called the free-electron final-state model because a free-electron dispersion relation is assumed for the final-state photoelectron in the solid. The refraction effect is included by shifting the dispersion relation in energy by the inner potential V_o:[48]

$$E(|k^f|) = \frac{\hbar^2|k^f|^2}{2m} - V_0 \qquad (4)$$

Conservation of energy in the photoexcitation event requires:[48]

$$h\nu - E_{IN} - \phi = E(|k^f|) \qquad (5)$$

where E_{IN} is the binding energy (≥ 0) of the initial state with respect to E_F; ϕ is the metal's work function (4.6 eV for Cr(001)) and hν is the photon energy. Energy is conserved as the photoelectron passes the surface and enters the vacuum:[48]

$$E(|k^f|) = \frac{\hbar^2|k^f|^2}{2m} - V_0 = \frac{\hbar^2|p^f|^2}{2m} = E(|p^f|) \qquad (6)$$

Refraction does not affect the final-state wavevector component parallel to the surface $k_{\parallel}^f$, so that in the absence of surface umklapping:[48]

$$k_{\parallel}^f = p_{\parallel}^f \qquad (7)$$

From the relationships (4)-(7) kinematic equations for the components $k_\perp^f$ ($Å^{-1}$) and $k_\parallel^f$ ($Å^{-1}$) of the final-state momentum in the solid can be derived:[49]

$$k_\perp^f = .512\ [(h\nu - E_{IN} - \phi)\ \cos^2\theta_e + V_0]^{1/2} \qquad (8)$$

$$k_\parallel^f = .512\ (h\nu - E_{IN} - \phi)^{1/2}\ \sin\theta_e \qquad (9)$$

Here θ_e is the angle of electron detection with respect to the surface normal, as shown in Fig. 4. With $\underset{\sim}{k}^f$ of the spectral peak determined, relation (1) is used to assign the value $\underset{\sim}{k}_i$ to the initial state responsible for the peak in the ARPES spectrum.

The inner potential V_0 can often be determined by normal-emission ($\theta_e = 0°$) ARPES measurements of $k_\perp^f$. The value of V_0 is adjusted so that eqn. (8) yields initial-state dispersions that are symmetric about the theoretical Brillouin zone center or boundary.[2,20,49] Results for V_0 obtained in this way usually agree well with the theoretical values of V_0 taken as the energy difference between the vacuum level and the bottom of the S band.[2,20,49] We were unable to make UPS measurements over the required photon energy range to permit a determination of V_0. Consequently, we assumed for V_0 the value chosen by Gewinner et. al.[41] (10.8 eV) with the hope that final-state momentum broadening (discussed below) would make an exact knowledge of V_0 unnecessary. As we shall show, subsequent normal-emission SXPS measurements suggest that the value 10.8 eV is probably close to the

correct value for V_o.

The established validity of eqns. (8) and (9) allows one to base an experiment on them.[49] The first objective of our experiments is to probe Cr initial states whose $\underset{\sim}{k}_i$ lie parallel to the surface along the [010] $\Gamma(H)$-X-$\Gamma(\Gamma)$ symmetry line in the first Brillouin zone. To observe such initial states in a photoelectric transition, the DTM (eqn. (1)) requires $\underset{\sim}{k}^f$ to lie on a parallel final-state [010] $\Gamma(H)$-X-$\Gamma(\Gamma)$ line in a higher Brillouin zone. The photon energies available for our UPS measurements required that we use the [010] $\Gamma(H)$-X-$\Gamma(\Gamma)$ final-state line in the second Brillouin zone. This is indicated by the solid line in Fig. 5(a) for the PM Brillouin zone, and by the dashed line in Fig. 5(b) for the AF Brillouin zone. All $\underset{\sim}{k}^f$ on this line have $k_\perp^f = 2.18$ Å^{-1}.

Suppose we suspect (from a theoretical band structure for commensurate AF Cr) the existence of an initial state with binding energy near E_{IN} and wavevector near $\underset{\sim}{k}_i$. Equations (8) and (9) can be used to calculate the hν and θ_e necessary to observe this suspected band state because we know the $\underset{\sim}{k}^f$ required by the DTM. Note that synchrotron radiation is required. As stated above, for our UPS measurements $k_\perp^f = 2.18$ Å^{-1}. The component $k_\parallel^f$ is then chosen so that $\underset{\sim}{k}^f$ probes the $\underset{\sim}{k}_i$ of interest. The required hν and θ_e are then calculated and the spectrum is taken. The appearance of a peak in the ARPES spectrum near E_{IN} confirms our original suspicion. The measured E_{IN} is then used with hν and θ_e in eqns. (8) and (9) to calculate the $k_\perp^f$ and $k_\parallel^f$ of the observed photoelectron

peak. Equation (1) is then used to determine $\underset{\sim}{k}_i$.

If the observed E_{IN} differs substantially from the suspected E_{IN}, then the observed $k_\perp^f$ may deviate significantly from 2.18 $Å^{-1}$. Fortunately, the k-space resolution of ARPES is finite. Inelastic scattering of the photoelectron introduces an intrinsic final-state momentum broadening Δk^f. An estimate of this broadening based on the photoelectron mean free path[50] gives $\Delta k^f = \pm 0.06$ $Å^{-1}$. An extrinsic constraint on momentum resolution is the acceptance angle ($\pm 3^\circ$) of our electron analyser. For the off-normal UPS measurements, the total k-space resolution, Δk^{tot} is estimated to be ± 0.12 $Å^{-1}$. This is shown as a box around the tip of $\underset{\sim}{k}^f$ in Fig. 5(b). As a consequence of this broadening, UPS spectral peaks whose $k_\perp^f$ values are within $\pm$ 6 percent of 2.18 $Å^{-1}$ can be viewed as arising from initial states along the [010] Γ(H)-X-Γ(Γ) symmetry line. For the SXPS spectra, Δk^f is estimated to be ± 0.10 $Å^{-1}$. In the normal-emission geometry, the finite angular resolution degrades the extrinsic $k_\parallel$ resolution. Consequently, for the SXPS measurements, $\Delta k_\parallel^{tot} \sim \pm 0.25$ $Å^{-1}$, and $\Delta k_\perp^{tot} \sim \pm 0.10$ $Å^{-1}$.

IV. RESULTS

Figure 6 displays five UPS spectra out of 50 that were taken of Cr(001) (at 298 K) to probe the [010] Γ(H)-X-Γ(Γ) line for binding energy (E_{IN}) values of 2 - 4 eV. The value $k_\parallel^f$ ($Å^{-1}$) is the magnitude of the parallel component (along [010]) of the final-state

wavevector for the peak marked with a tic. We use the DTM (eqn. (1)) to associate $k_{\|}^{f}$ with an initial-state wavevector $\underset{\sim}{k}_i$ along the [010] Γ(H)-X-Γ(Γ) symmetry line in the first Brillouin zone. For the PM Brillouin zone of Fig. 5(a), $k_{\|}^{f} = 0$ probes $\underset{\sim}{k}_i$ at the (H) point since $k_{\perp}^{f}$ is chosen to be 2.18 Å^{-1}. When viewed in the AF Brillouin zone of Fig. 5(b), direct transitions to $k_{\|}^{f} = 0$ arise from $\underset{\sim}{k}_i$ at the Γ point. Note in Fig. 6 how the marked peak disperses away from E_F as $k_{\|}^{f}$ increases. It attains maximum binding energy at $k_{\|}^{f} =$ 1.07(8) Å^{-1}. As $k_{\|}^{f}$ increases beyond 1.07(8) Å^{-1}, the spectra become dominated by a high-intensity feature at $0.6 \leq E_{IN} \leq 0.9$ eV. Despite the increased background, the marked peak is still observable. For $k_{\|}^{f} > 1.07(8)$ Å^{-1}, it disperses back toward E_F.

Figure 7 plots E_{IN} versus $k_{\|}^{f}$ along Γ(H)-X-Γ(Γ) for the features observed in our UPS spectra. Three distinct bands of points are present. Band III is the high-intensity initial state of Fig. 6. It is observed for $1.0 \leq k_{\|}^{f} \leq 2.0$ Å^{-1}, and disperses from $E_{IN} \sim 0.9$ eV to ~ 0.6 eV. Figure 8 displays the sharp onset of Band III at $k_{\|}^{f} \sim$ 1.0 Å^{-1}. As $k_{\|}^{f}$ increases, the Band III photoelectron peak grows in intensity. Figure 9 displays Band III's remarkable sensitivity to surface contamination. The Band III feature at $E_{IN} = 0.70(5)$ eV with $k_{\|}^{f} = 1.33(8)$ Å^{-1} is strongly attenuated by exposing the Cr(001) surface to 1 L of CO. This suggests that Band III is a feature of the surface electronic structure. The existence of Band III inhibits the study of near-surface Cr(001) electronic structure

for the region of $k_{\|}^{f}$ and E_{IN} over which it is present. We defer a complete discussion of the origin and characteristics of this surface feature to a future publication.

Band II is located at E_{IN} = 2.4(1) eV for $k_{\|}^{f}$ = 0.15(8) $Å^{-1}$ in Fig. 7. As $k_{\|}^{f}$ increases, Band II disperses toward E_F. At $k_{\|}^{f}$ ~ 1.06(8) $Å^{-1}$, Band II suddenly flattens out, with E_{IN} = 1.5(1) eV. Band I is the valence band sampled by the marked peaks in the spectra of Fig. 6. At $k_{\|}^{f}$ = 0.20(8) $Å^{-1}$, E_{IN} = 3.2(1) eV for Band I. As $k_{\|}^{f}$ increases, E_{IN} increases to a maximum of 4.1(1) eV at $k_{\|}^{f}$ = 1.07(8) $Å^{-1}$. This value of $k_{\|}^{f}$ corresponds to the X point (1.09 $Å^{-1}$) of the theoretical AF Brillouin zone (Fig. 2) to within the experimental uncertainty. As $k_{\|}^{f}$ increases beyond 1.07(8) $Å^{-1}$, Band I disperses symmetrically back toward E_F. In contrast to Band III, Bands I and II show negligible sensitivity to surface contamination. This suggests that Bands I and II arise from the Cr(001) near-surface electronic structure.

The smooth symmetrical dispersion of Band I about the X point in Fig. 7 is strong evidence that the X point is a Brillouin zone boundary for the [010] near-surface electronic structure. This periodicity is only consistent with that expected for an AF electronic structure, Fig. 3(b). The periodicity of Band I's dispersion is certainly inconsistent with our expectations for a PM phase, Fig. 3(a). We therefore interpret the dispersion of Band I in Fig. 7 as evidence that the near-surface valence electrons feel, and self-consistently establish, antiferromagnetism in the near-surface layers of Cr(001). This conclusion is also consistent with the

flattening of Band II at the X point, although the absence of symmetrical dispersion for Band II is not understood. These properties suggest that the near-surface electronic structure of Cr(001) along the [010] direction should be described in the sc Brillouin zone of the AF state. This result implies that simple cubic symmetry is at least approximately realized along the [001] direction. This remains to be evaluated. However, we can conclude that the AF Brillouin zone, Fig. 5(b), and not the PM Brillouin zone, Fig. 5(a), gives the more appropriate description of the DTM as it applies to our ARPES investigation of Cr(001). We now discontinue the dual notation $\Gamma(\Gamma)$ and $\Gamma(H)$, and hereafter refer to this point as Γ, as shown at the top of Fig 7. The magnitude $k_{\parallel}^{f}$ can now be equated with $\underset{\sim}{k}_{i}$ along [010] (Fig. 5(b)), and is hereafter referred to simply as $k_{\parallel}$.

The lines graphed in Fig. 7 are the theoretical Γ-X-Γ dispersion relations for commensurate AF bulk chromium, as calculated by Skriver.[30] The experimental and theoretical X point critical binding energies are in excellent agreement. Within $\pm$ 0.4 Å^{-1} of the X point, Band I is predicted very well by the theory. However, for Band II just off the X point and for both Band I and Band II with $k_{\parallel} < 0.5$ Å^{-1}, experiment and theory agree poorly. An interesting aspect of Fig. 7 is that Bands I and II remain split very near the Γ point. Figure 10 shows the persistence of this splitting for peaks with $k_{\parallel}$ near Γ. In the theory, these valence bands are essentially degenerate for $k_{\parallel} \leq 0.3$ Å^{-1}.

The off-normal UPS measurements probe the [010] Γ-X-Γ line parallel to the surface. We have also collected normal-emission ARPES spectra at 298 K using soft x-ray photons of energy $80 \leq h\nu \leq 150$ eV. These SXPS spectra probe the [001] Γ-X-Γ symmetry line perpendicular to the surface by detecting only those $\underset{\sim}{k}^f$ that lie along the [001] Γ-X-Γ line in the third Brillouin zone. Since $k_{\|}^f = 0$, all near-surface spectral features arise from [001] Γ-X-Γ initial states in the first Brillouin zone. Figure 11 displays five SXPS spectra. For $h\nu \leq 105$ eV, strong transitions arise from surface-related states that produce photoelectron peaks with $E_{IN} < 1$ eV. As the photon energy is increased, the prominence of both surface features decreases, and that of the marked near-surface peak increases. Figure 12 emphasizes these intensity variations by directly comparing SXPS spectra collected with $h\nu = 80.0$ eV and $h\nu = 130.0$ eV.

The $k_\perp$ value associated with each spectrum in Figs. 11 and 12 is the magnitude of the wavevector $\underset{\sim}{k}_i$ (along [001]) of the initial state producing the spectrum's near-surface photoelectron peak. This was calculated from eqn. (8) using $V_o = 10.8$ eV, and eqn. (1). The value $k_\perp = 0$ corresponds to the Γ point. Figure 11 demonstrates that as $k_\perp$ for the near-surface peak increases, the feature disperses away from E_F. It attains a maximum binding energy of $E_{IN} = 3.7(1)$ eV at $k_\perp = 0.94(8)$ Å^{-1}. For $k_\perp \geq 0.94(8)$ Å^{-1}, the near-surface feature disperses symmetrically back toward E_F.

Unlike the UPS measurements, the position of the band minimum observed in our SXPS measurements depends on our assignment of the

$k_\perp^f$ values, and hence on V_o through eqn. (8). We have plotted in Fig. 13 the near-surface E_{IN} vs. $k_\perp$ results from our SXPS spectra. In doing so, we have recalculated the $k_\perp$ values using V_o = 16.6 eV in eqn. (8). This choice of V_o shifts the position of the band minimum from 0.94(8) $Å^{-1}$ (V_o = 10.8 eV) to the theoretical bulk X point. This shift was made only to clarify Fig. 13's comparison of the experimentally observed band shape to the theoretical bulk dispersion relations. There is a similarity between the shape of the band dispersion, Skriver's theoretical prediction (the lines in Fig. 13) and the UPS results (Fig. 7). This suggests that the band observed in the SXPS spectra and plotted in Fig. 13 is the [001] Γ-X-Γ analogue to the Band I observed along the [010] Γ-X-Γ line in the UPS measurements. The dispersion of Band I in Fig. 13 is shallower than that shown in Fig. 7. Figures 7 and 13 also differ by ~ 0.25 eV for the binding energy of Band I near the Γ point.

The value V_o = 16.6 eV required to make the SXPS Band I dispersion symmetrical about the [001] X point is rather large. The theoretical value of V_o (derived from Skriver's AF Cr band structure) is 12.6 eV. ARPES investigations[2,20] of other transition metals have reported values for V_o in the range 12 - 14 eV. This indicates that the true point of symmetrical band dispersion is not the X point for $\underset{\sim}{k}_i$ along [001]. The fact that Band I disperses symmetrically about a point near the [001] X point is an indication that antiferromagnetism exists in the near-surface region of Cr(001). This is the same conclusion that was drawn from our UPS results for

the [010] electronic structure. However, in contrast to the [010] direction, the observed periodicity of the [001] band dispersions is different than that expected for presumably indistinguishable commensurate (Fig. 3(b)) or incommensurate (Fig. 3(c)) AF states.

It must be emphasized that the mean free path for the SXPS photoelectrons is particularly small, only ~5 Å[51] or 4 atomic layers. It will become clear in Section V that when the [001] electronic structure is investigated with such high surface sensitivity, a result differing from that obtained for the [010] direction is not alarming. Consequently, we will only conclude that a value of V_o a little higher than 10.8 eV, perhaps ~ 13 eV, might be more suitable for the interpretation of the ARPES measurements. This possibility has only a six percent effect on the inferred values of $k_\perp^f$ for our UPS spectra. It has no effect on the inferred $k_\parallel^f$ values. The position of the Band I dispersion in Fig. 7 is independent of the choice of V_o.

The comparison of the UPS and SXPS results with bulk AF theory suggests that Band I belongs to the Δ_1 representation and Band II to the Δ_2 representation of the C_{4V} point group. Both representations are even with respect to reflection through the (100) mirror plane containing the photoelectron and photon polarization vectors (Fig. 4). Hence, both are allowed by the symmetry selection rules governing our off-normal UPS measurements.[15] The symmetry of Band I is revealed in Fig. 14. The UPS spectrum 14(a) was recorded in the normal-emission geometry ($\theta_e = 0°$ in Fig. 4). The peak at

E_{IN} = 3.25(5) eV arises from a Band I initial state with $\underset{\sim}{k}_i$ = 0.34(8) $Å^{-1}$ along [001]. For this P-polarization geometry, only Δ_1 and Δ_5 initial states are allowed.[15] That Band I has Δ_1 symmetry is shown by spectrum 14(b). For 14(b) the $\underset{\sim}{A}$ vector has been rotated to lie on the surface along the [100] direction. For this S-polarization geometry, only Δ_5 initial states are allowed.[15] The strong suppression of the Band I photoelectron peak indicates that Band I has Δ_1 symmetry. Spectra 14(c) and 14(d) present a similar test for Band I, only for E_{IN} = 4.15(5) eV at $k_{||}$ = 1.18(8) $Å^{-1}$. These two spectra show that at this $k_{||}$, Band I is even with respect to reflection through the (100) mirror plane. This is consistent with the assignment of Δ_1 symmetry.

It is interesting to compare spectrum 14(a) with the $\theta_e = 9°$ spectrum of Fig. 10. Both spectra probe Γ-X-Γ lines near 0.3 $Å^{-1}$. However, Band II is observed only in the off-normal measurement of Fig. 10. This shows that Band II has Δ_2 symmetry because Δ_2 initial states are symmetry allowed in the P-polarization off-normal measurements, but are symmetry forbidden in the normal-emission geometry. Note that the higher-energy normal-emission SXPS measurements are also consistent with these symmetry assignments. Only Band I of Δ_1 symmetry is observed. Band II of Δ_2 symmetry is absent, as shown in Fig. 13.

Almost all of the near-surface spectral features observed in our ARPES measurements of Cr(001) can be interpreted as direct transitions from AF initial states along the Γ-X-Γ symmetry line. However, Fig. 7

displays a cluster of low-intensity peaks at $E_{IN} \sim 2.3$ eV and $k_{\parallel} \sim 1.1$ Å^{-1} that has no theoretical counterpart. Their binding energy coincides with that of Band II near Γ. We speculate that these weak peaks are produced by final-state scattering that results in a type of nondirect transition (NDT) from the high density of states region of Band II near Γ. As such, they would have Δ_2 symmetry. The fact that they are <u>not</u> observed in the normal-emission SXPS measurements (Fig. 13) is consistent with this conjecture. Similarly, a NDT feature of Δ_1 symmetry might arise from the high density of states region of Band I near ~ 3 eV binding energy. We tentatively interpret the shoulder in spectrum (c) of Fig. 14 with $E_{IN} = 3.0(2)$ eV as such a NDT feature. This feature is even with respect to reflection through the (100) mirror plane, as shown by its absence in spectrum 14(d). This supports our expectation of Δ_1 symmetry. The physical origin of these NDT peaks is not well understood.

The temperature dependence of antiferromagnetic properties are of fundamental interest. We have therefore investigated the influence of temperature on the [010] AF energy bands observed in our UPS measurements. The symmetrical dispersion of Band I about the X point in Fig. 7 is a manifestation of antiferromagnetism in the near-surface region of Cr(001). More specifically, the existence of Band I with $3.0 \leq E_{IN} \leq 4.1$ eV and $k_{\parallel} > 1.09$ Å^{-1} (X point) is a property of the AF state that distinguishes it from our expectations for the PM electronic structure. In contrast, the existence of Band I with $3.0 \leq E_{IN} \leq 4.1$ eV and $k_{\parallel} \leq 1.09$ Å^{-1} is possible for both the AF

and PM phases. That it is possible for the PM phase can be understood by referring to a PM band calculation and interpreting the photoemission in the PM Brillouin zone of Fig. 5(a). A priori, one might expect the bulk Néel temperature, T_N = 312 K, to mark a sharp transition between well-defined near-surface AF and PM phases. For $T > T_N$, one might then expect the persistence of those Band I spectral features with $k_{\|} < 1.09$ Å^{-1}, and the disappearance of those Band I peaks with $k_{\|} > 1.09$ Å^{-1}. Figure 15 presents ARPES spectra taken at temperatures as high as 670 degrees above T_N. There is almost no change with temperature in the appearance of the Band I peak at E_{IN} = 3.32(5) eV; $k_{\|}$ = 0.72(8) Å^{-1}. The only spectral change occurs for Band II and then only for T ~ 980 K. These observations are consistent with the above expectations for Band I.

Figure 16 displays ARPES spectra that sample Band I at E_{IN} = 3.07(5) eV; $k_{\|}$ = 1.64(8) Å^{-1}. Contrary to our hypothesis, Band I is still observed as high as 500 degrees above the bulk Néel temperature, although the intensity of the spectral peak is reduced from that observed at 298 K. For the spectrum taken in the range $955 \leq T \leq 1130$ K there is evidence for the expected disappearance of Band I. We interpret the persistence of Band I in Fig. 16 as a clear indication of near-surface antiferromagnetic order in Cr(001) for $T \leq 2.5\ T_N$. The highest temperature spectrum suggests that this order is disrupted at 3.3 T_N.

As described in Section I, phonon-assisted NDT can degrade the k-space resolution of high-temperature ARPES spectra. The realized

percentage of direct transitions can be estimated from the Debye-Waller factor, eqn. (2). For chromium at T = 1000 K, we estimate $\%\,DT \sim 95$ percent. The highest temperature spectra of Figs. 15 and 16 thus contain the largest contribution from phonon-assisted NDT. For these spectra, it constitutes a ~ 5 percent effect.

V. DISCUSSION

A discussion of these results must consider the influence of surface ferromagnetism on the Cr(001) near-surface electronic structure. Experiment[35] has confirmed the theoretical prediction[36-39] of a ferromagnetic surface phase on Cr(001). Theoretically, the relatively small number of nearest-neighbors (4) for the (001) surface atoms leads to energy-band narrowing, resulting in the formation of large ($\sim 2.7\mu_B$) localized surface magnetic moments. The surface ferromagnetism is characterized by an exchange-split surface spin density of states, SSDOS. A surface-related feature (hereafter referred to as the surface feature 2) was observed in normal-emission ARPES and assigned to the majority SSDOS.[35] The temperature dependence of its binding energy signals a surface magnetic phase transition on Cr(001) near 780 K.[35]

Since the number of nearest neighbors (8) is already bulklike for the second-layer atoms, the Cr(001) surface ferromagnetism is expected to be highly surface-localized. However, several near-surface layers

must be encompassed by the decrease of the magnetic moment to the maximum bulk value of 0.59 μ_B. Allan[38] has predicted that the magnitude of the magnetic moment on layer l, M(l), differs from that of the bulk according to:

$$\frac{M(l)-M(bulk)}{M(0)-M(bulk)} \sim \exp(-l/l_0) \qquad (10)$$

where $l_0 = 1.67$ in units of the interplanar spacing. If the surface layer has $M(0) = 2.7\mu_B$ then this model predicts that 5 layers into the surface, $M(4) = 0.8\mu_B$. This magnitude still deviates significantly from the maximum bulk value.

These expectations for Cr(001) surface and near-surface magnetism are presented in Fig. 17. In this figure, the diameter of the sphere representing an atom is drawn proportional to the atom's magnetic moment as predicted by eqn. (10). The sign of the sublattice magnetization is expected to alternate along both the [001] and [010] directions. Hence, the near-surface region is predicted to be antiferromagnetic. However, the Cr(001) surface ferromagnetism would distinguish between the [001] and the [010] directions. Along the [010] direction, the atomic magnetic moment is not changing in magnitude. Thus, parallel to the (001) surface, the near-surface antiferromagnetism is predicted to be <u>commensurate</u> with the crystal lattice. Along the [001] direction, the magnitude of the magnetic moment is expected to change according to eqn. (10). We emphasize that this layer-dependent magnetization profile is conceptually distinct from the incommensurate SDW magnetization that exists in bulk

chromium. The near-surface magnetic properties are thought to be completely determined by the ferromagnetism of the Cr(001) surface.[36,38]

We have already cited the experimental evidence[35] for a ferromagnetic surface phase on Cr(001). We now show that our results for the Cr(001) near-surface electronic structure are consistent with the theoretical predictions for Cr(001) near-surface magnetism. The band dispersions observed in our UPS spectra and presented in Fig. 7 show that the sc Brillouin zone describes the periodicity of the valence electronic structure along the [010] direction. This is consistent with a commensurate AF spin density along [010], as depicted in Fig. 17. Our SXPS measurements revealed the dispersion of Band I about a position near the [001] X point (Fig. 13). This suggests that within the first four layers, an AF spin density (not necessarily of simple cubic symmetry) obtains along the [001] direction. This is strong evidence that the surface magnetic moments, while coupling ferromagnetically to each other within the surface layer, couple antiferromagnetically to the moments of the second-layer atoms, as shown in Fig. 17. These SXPS results reveal a single well-defined band (Band I) that fails to disperse symmetrically about the [001] X point when physically reasonable values are assumed for the inner potential V_o. This dispersive behavior is inconsistent with the (spectroscopically indistinguishable) energy-band periodicity expected for commensurate (Fig. 3(b)) and incommensurate (Fig. 3(c)) antiferromagnetism. We speculate that the observed behavior might in

some way reflect a reduced symmetry along the [001] direction in the near-surface layers of Cr(001). A likely contribution to this reduced symmetry would be the decreasing magnetization along the [001] direction postulated in Fig. 17. If this interpretation is correct, then simple cubic symmetry may be only approximately realized along the [001] direction. If so, then the depiction of wavevector conservation in Fig. 5(b) is only approximately correct, for Fig. 5(b) involves exact simple cubic symmetry along the [001] direction.

In stating our general expectations for AF electronic structure (Fig. 3(b)), we have not indicated the size of the energy gap created at the X point. Thus the strength with which the AF potential mixes the sinusoidal states $|k\rangle$ and $|k \pm 2\pi/a\rangle$ has not been specified. For an infinitesimal AF potential, the extra bands that distinguish antiferromagnetism (Fig. 3(b)) from paramagnetism (Fig. 3(a)) would manifest themselves as infinitely weak photoelectron peaks in our ARPES measurements. For a real AF system, one would expect these bands to produce ARPES features with a considerably reduced relative intensity. The UPS observation of Band I with $3.0 \leq E_{IN} \leq 4.1$ eV and $k_{\|} \geq 1.09$ Å^{-1} signals the existence of antiferromagnetism in the Cr(001) near-surface layers. However, the existence of Band I with $3.0 \leq E_{IN} \leq 4.1$ eV and $k_{\|} \leq 1.09$ Å^{-1} is not a determining property, since it is consistent with either a PM or an AF state. An attempt was made to contrast the spectral intensities of Band I features with $k_{\|} \geq 1.09$ Å^{-1} (AF) and $k_{\|} \leq 1.09$ Å^{-1} (PM or AF). The prominence of Band I for $k_{\|} \geq 1.09$ Å^{-1} (AF) is considerably

reduced relative to that observed for $k_{\parallel} \leq 1.09$ Å^{-1} (PM or AF). However, angle- and hν-dependent variations in the spectral backgrounds as well as the absence of photon intensity measurements preclude a meaningful discussion of the relative Band I intensities observed in our UPS measurements.

The incident photon intensities were not measured for our SXPS data. Therefore, we cannot rigorously determine the variation of the Band I spectral intensity with $k_{\perp}$ from those results. However, the inelastic background intensity in the SXPS photoelectron spectra appeared to be well-behaved and varied slowly with photon energy. Consequently, we can use this background as an approximate normalization standard to make qualitative statements concerning the relative Band I intensities observed in our SXPS investigation. The existence of Band I with $3.5 \leq E_{IN} \leq 3.7$ eV and $k_{\perp} \leq 1.09$ Å^{-1} is the manifestation of antiferromagnetism in our SXPS results. This cannot be claimed for the observation of Band I with $k_{\perp} \geq 1.09$ Å^{-1}, since that observation is consistent with either a PM or an AF state. Figure 11 displays the increasing prominence of the marked Band I near-surface peak as $k_{\perp}$ is sampled from 0.57 Å^{-1} to 1.31 Å^{-1}. Figure 12 reveals directly that the Band I spectral intensity observed with $k_{\perp} = 0.30$ Å^{-1} (AF) is dramatically less than that observed with $k_{\perp} = 1.56$ Å^{-1} (PM or AF). Note that these near-surface initial states are equidistant in k-space from the observed Band I minimum at $k_{\perp} \sim 0.94$ Å^{-1}. The relative weakness of the Band I intensity for $k_{\perp} \leq 0.94$ Å^{-1} (AF) is qualitatively consistent with the reduced

spectral intensity expected for a photoelectron peak of AF origin.

The electronic structure of Cr at elevated temperature is of great interest. Bulk chromium undergoes a macroscopic SDW to PM phase transition at T_N = 312 K. This is observed as a cusp in the magnetic susceptibility at T_N. However, the theoretical description[52] of temperature-dependent linear expansion measurements[53] of Cr suggests that substantial and localized magnetic moments persist in the paramagnetic phase. Theoretically, these moments are not well-defined because they are believed to be fluctuating about zero magnitude.[52,54] However, the rms magnitude of these moments is reduced by only 3 percent from the values observed in the SDW phase.[52] Neutron diffraction measurements[23,24] of the paramagnetic phase have shown that these moments exist on at least the picosecond time scale, and that they are considerably correlated. Above T_N well-defined spin-wave excitations and elastic magnetic reflections have been observed.[23,24] Neither the Stoner (or Band) Model that predicts zero spin density above T_N, nor the Heisenberg (or Local) Model that predicts totally randomized local magnetic moments above T_N can account for the existence of such phenomena in the paramagnetic phase of chromium.

The Local Band Theories[55-70] were developed to explain similar spin-correlation phenomena in itinerant ferromagnets above the Curie temperature, T_C. In their general application, the Local Band Theories introduce localized magnetic moments whose magnitudes and relative orientation can change with temperature by itinerant

effects. The result is an itinerant paramagnetic state that consists of transverse spin waves composed of localized magnetic moments. The disordering of these moments produces a reduction of the moments' magnitude from the value found below the transition temperature. Within several unit cells, the moments are sufficiently correlated to permit a short-range magnetic order. However, the spin waves destroy the long-range alignment of the moments between cells, and with it, long-range magnetic order. Remaining questions concern the spatial extent of the magnetic order at a given temperature and the manner in which the moment magnitudes and directions fluctuate with time.

Of particular relevance to our work are Grempel's spin-fluctuation calculations of the temperature-dependent surface magnetic ordering on Cr(001).[36] His theoretical surface magnetic phase transition temperature T_S = 850 K, and surface magnetic moment $M_S = 2.6\mu_B$ are near the values $T_S \sim 780$ K and $M_S \sim 2\mu_B$ inferred in our previous paper.[35] Grempel also calculated the magnetization profile as a function of temperature.[36] His results predict that the high thermal stability of the surface ferromagnetic phase will hold the near-surface region of Cr(001) antiferromagnetic well above T_N. In spin-fluctuation theory, a decrease in magnetization occurs via the thermal population of spin configurations for which the moments are <u>disordered</u> and possibly reduced in magnitude to some extent. Grempel predicts only a ~ 10% decrease in the surface local band splitting (e.g. in the <u>magnitude</u> of the surface magnetic moment) during the surface magnetic phase transition. This particular

prediction is not quantitatively supported by our previous results[35] for the surface feature 2 that reveal a marked decrease in the local surface magnetization for temperatures approaching T_s. Grempel's work remains the only theoretical treatment of the temperature-dependent magnetization of the Cr(001) surface.

The observation of Band I in Fig. 16 for $T \leq 2.5\ T_N$ indicates the existence of AF order in the Cr(001) near-surface region well above the bulk Néel temperature. Since we observe this order via ARPES, we estimate the spatial extent of the AF order to be at least ~ 15 Å.[71] There are at least two possible causes of this phenomenon. The first stems from Grempel's calculation. As described previously, the thermal stability of the AF order in the near-surface layers might be largely determined by the Cr(001) surface ferromagnetism. The persistence of AF order well above T_N might then be viewed as an AF order induced in the Cr(001) near-surface region by the ferromagnetism of the Cr(001) surface below T_s. We believe that the temperature dependence of feature 2's binding energy is a manifestation of the thermal decrease of the local surface exchange potential, and therefore, the local surface magnetization.[35] If the near-surface AF order observed above T_N were induced solely by the ferromagnetism of the surface, then one would expect a correlation between the temperature dependence of the Band I intensity in Fig. 16, and the thermal decrease of feature 2's binding energy. We make such a comparison in Fig. 18. The two properties do show a gross similarity. If our interpretation of the

feature 2 is correct, then by 600 K, M_s has decreased by at least 40 percent. Despite this reduction of the local surface magnetization, Band I (and therefore local AF order) is still observed. It may be that the remnant surface magnetism can induce a residual near-surface AF order at this temperature. Only for the highest temperatures is this AF order completely disrupted, as suggested by Fig. 18.

A second explanation of the observed AF order at high temperatures does not consider it to be a near-surface phenomenon. As discussed above, temperature-dependent linear expansion measurements[53] of bulk Cr are consistent with the existence of substantial, though probably fluctuating, local magnetic moments in the paramagnetic phase.[52,54] Neutron diffraction measurements[23,24] have shown that as high as 100 K above T_N, these moments exist on the picosecond time scale, and are highly correlated. Our ARPES measurement is a much faster (10^{-16} sec.) and much more local (~15 Å) probe of the magnetic structure than neutron diffraction. Consequently, the near-surface AF order observed at temperatures as high as 500 K above T_N (Fig. 18) might result from a local AF coupling of essentially bulklike magnetic moments. This coupling could be capable of producing AF order within a range of ~ 15 Å at $T = 2.5\ T_N$, but not for temperatures as high as $3.3\ T_N$, as indicated by Fig. 18. In this way, short-range AF order even deep in the bulk would become consistent with the macroscopic (long-range) paramagnetism of bulk chromium at $2.5\ T_N$. The overall correlation shown in Fig. 18 would

then be considered coincidental. Such short-range AF order in Cr above T_N might then have a description in the Local Band Theories.

It seems likely that the physics of both of these explanations are operative. Thus we believe that the near-surface AF order observed for temperatures up to 2.5 T_N is caused by the AF correlation of localized Cr magnetic moments. The strength of this interaction, and thereby the thermal stability of the near-surface AF order, is increased because the near-surface moments are enhanced due to the Cr(001) surface ferromagnetism.

Almost all of our experimental results confirm the theoretical belief[36,38] that the Cr(001) near-surface antiferromagnetism is perturbed primarily by the Cr(001) surface ferromagnetism, and not by those electronic effects responsible for the incommensurate periodicity of the SDW in the bulk. Thus along the [010] direction, the near-surface AF order is predicted to be commensurate with the crystal lattice, as depicted in Fig. 17. We have shown that this prediction is consistent with our UPS investigation of the [010] electronic structure. Unfortunately it cannot be proven because commensurate (Fig. 3(b)) and incommensurate (Fig. 3(c)) antiferromagnetic band dispersions may be spectroscopically indistinguishable. However, our ARPES results are consistent with Fig. 17's portrayal of Cr(001) surface and near-surface magnetism. Consequently, we believe that the Cr(001) near-surface AF order is in fact commensurate with the crystal lattice along the [010] direction.

This finding justifies the comparison made in Fig. 7 between our

UPS [010] Γ-X-Γ results and Skriver's calculation for commensurate AF chromium.[30] The comparison is not completely appropriate because the moments in the near-surface region are expected to be enhanced. Skriver's theory for bulk AF chromium does not incorporate this complication. It is therefore not surprising that discrepancies exist between the bulk theory and our near-surface ARPES results, as shown in Fig. 7. The origin of some of these discrepancies will hopefully be elucidated in future theoretical work. The comparison made in Fig. 13 between the SXPS [001] Γ-X-Γ results and bulk AF theory is not in principle justified by symmetry, because there is evidence that a strictly simple cubic symmetry does not exist along the [001] direction. Nevertheless, the comparison aids in the qualitative identification of the band observed in the SXPS measurements.

A distinction is often made between surface and bulk electronic structure in ARPES investigations of metal surfaces. We have made a similar separation for Cr(001). In this work, we have considered Band I and Band II as representative of the near-surface electronic structure. In our previous paper[35], we assigned the surface feature 2 to the majority SSDOS. In view of the influence that the Cr(001) surface ferromagnetism may have on the near-surface electronic structure, the distinction between surface and near-surface properties may seem unclear. We point out that the surface feature 2 is highly sensitive to surface contamination. Neither Band I nor Band II shows significant sensitivity to CO decomposition on the Cr(001) surface. In addition, the temperature dependence of feature 2 is qualitatively

different than that of the AF bands observed in this work. The surface feature 2 displays a decrease in binding energy as the temperature is raised. In contrast, the Band I and Band II binding energies remain constant with temperature, as shown in Figs. 15 and 16. Thus in both surface sensitivity and temperature dependence, the surface feature 2 displays different characteristics than the AF initial states. It is by these properties that we differentiate between surface and near-surface electronic structure. This makes possible the assignment of feature 2 to the Cr(001) ferromagnetic surface electronic structure, and Bands I and II to the antiferromagnetic near-surface electronic structure.

VI. RELATIONSHIP TO PRIOR WORK

There have been two prior ARPES investigations of chromium near-surface electronic structure. Johansson et. al.[40] probed the ΓM symmetry line in normal-emission ARPES measurements of Cr(110). However, ARPES spectra of Cr(110) recently published by Wincott et. al.[72], as well as our own data for the (110) surface reveal that the results of Ref. 40 are influenced by surface contamination. The features reported at E_{IN} ~6 eV and ~3 eV in Ref. 40 are not present in spectra of the clean surface. We feel that such surface contamination prohibits a comparison of the results of Johansson et. al. with our investigation of clean Cr(001) electronic structure.

Gewinner and co-workers[41] made a previous ARPES study of

Cr(001). Using a helium discharge lamp ($h\nu$ = 21.22 eV) they attempted to probe the [010] symmetry line in off-normal ARPES. They interpreted the wavevector conservation of the photoemission process in the PM Brillouin zone (Fig. 5(a)). They also observed initial states whose dispersions seemed consistent with those calculated for the energy bands of the paramagnetic phase. Our results have shown that the AF Brillouin zone is the more appropriate structure for the description of both wavevector conservation in the photoemisssion process (Fig. 5(b)), and the dispersion of the initial states along the [010] direction. The valence bands are thus antiferromagnetic in nature.

One difference between our work and that of Ref. 41 is the level of surface cleanliness. Reference 41 reports a photoelectron peak at 6.7 eV binding energy that is absent in our spectra of clean Cr(001). This feature is due to impurity (oxygen and carbon) 2p photoemission. Its presence signals surface contamination by CO decomposition, as shown in Fig. 9. However, our study indicates that the near-surface AF electronic structure is not drastically affected by the small amounts of impurity necessary to produce this spectral peak.

We feel that the inability of Gewinner et. al. to observe the AF characteristics of the Cr(001) electronic structure probably stems from the fact that they did not use tunable synchrotron radiation in their off-normal ARPES study.[41] We emphasize that both our study and theirs use the same kinematic equations (8) and (9) to infer the values of the the final-state wavevector components $k_{\perp}^{f}$ and

$k_{\parallel}^{f}$. However, in contrast to Ref. 41, we were able to tune the photon energy so that we were always probing the initial-state $\underset{\sim}{k}_i$ of interest with $\underset{\sim}{k}^f$ on the Γ-X-Γ line, as described in Section III. This may be particularly necessary to observe the Band I features with $k_{\parallel} > 1.09$ Å^{-1} that are unique to the antiferromagnetic phase. In this region of k-space, the spectral intensity of Band I is expected to be intrinsically low due to its magnetic origin. Band I's prominence is further reduced for $k_{\parallel} > 1.09$ Å^{-1} by the spectral dominance of the high-intensity surface feature that we have called Band III. Differences between our data for Band II and the results of Ref. 41 may have a similar origin. The possible underestimate of the inner potential V_o, as discussed in Section IV, also emphasizes the need for synchrotron radiation if eqns. (8) and (9) are to be used accurately in the investigation of near-surface electronic structure.

We point out that the incorrect conclusions reported in Refs. 41 and 42 regarding the near-surface Cr(001) electronic structure have implications for their interpretation of Cr(001) surface electronic features. For instance, they assign a surface feature to a Δ_1 symmetry surface state located in a Δ_1 symmetry gap of the bulk paramagnetic band structure. The results that we have presented suggest that this assignment is not correct. In a future publication we will show that this surface feature (referred to in our work as the surface feature 2) has a different origin.

VII. CONCLUSIONS

We conclude by recalling the major results of our investigation of Cr(001) near-surface electronic structure.

1. Our UPS measurements revealed the periodicity of the valence-band dispersions along the [010] direction parallel to the crystal surface. The results indicate that the valence electrons feel, and self-consistently establish, antiferromagnetism in the Cr(001) near-surface layers. With respect to the [010] direction, this near-surface antiferromagnetism appears to possess simple cubic symmetry.

2. The agreement between these UPS results and theory for bulk commensurate AF chromium[30] is good near the X point. Agreement is poor near the Γ point.

3. The periodicity of the valence-band dispersions along the [001] direction normal to the crystal surface were measured in our SXPS investigation. The results are consistent with an AF spin arrangement within the first 4 atomic layers. This strongly suggests that the surface magnetic moments, which couple ferromagnetically to each other within the surface layer, couple antiferromagnetically to the magnetic moments of the second-layer atoms. However, the periodicity of the [001] band dispersions indicates that this near-surface antiferromagnetism <u>does not</u> possess purely simple cubic symmetry along the [001] direction.

4. The temperature dependence of the [010] near-surface AF

electronic structure was investigated. The results (Figs. 16 and 18) suggest that near-surface AF order persists on at least a local scale of ~ 15 Å for temperatures up to 2.5 T_N. This order is disrupted at $T = 3.3\ T_N$. The temperature dependence of the AF Band I intensity (Fig. 18) correlates to some extent with the decrease in the local surface ferromagnetism that we reported previously.[35] We interpret this correlation as evidence that the thermal stability of the near-surface AF order is determined in part by the ferromagnetism of the Cr(001) surface.

Acknowledgements

This work was supported by the Director, Office of Energy Research, Office of Basic Energy Sciences, Chemical Sciences Division of the U.S. Department of Energy under Contract No. DE-AC03-76SF00098. It was performed in part at the Stanford Synchrotron Radiation Laboratory, which is supported by the Department of Energy, Office of Basic Energy Sciences and the National Science Foundation, Division of Materials Research. Thanks are extended to John Barton and Charlie Bahr, both of whom provided invaluable assistance during the experiment. We are grateful to L.M Falicov, R.H. Victora and L.C. Davis for very helpful discussions. Discussions with G. Shirane of the measurements reported in Ref. 23 are greatly appreciated. We thank H.L. Skriver for supplying a listing of his theoretical AF Cr band structure.

REFERENCES

1. Z. Hussain, S. Kono, L.-G. Petersson, C.S. Fadley, and L.F. Wagner, Phys. Rev. B 23, 724 (1981).

2. P. Thiry, D. Chandesris, J. Lecante, C. Guillot, R. Pinchaux, and Y. Pétroff, Phys. Rev. Lett. 43, 82 (1979).

3. J.A. Knapp, F.J. Himpsel, and D.E. Eastman, Phys. Rev. B 19, 4952 (1979).

4. D.E. Eastman, J.A. Knapp, and F.J. Himpsel, Phys. Rev. Lett 41, 825 (1978).

5. J. Stöhr, P.S. Wehner, R.S. Williams, G. Apai, and D.A. Shirley, Phys. Rev. B 17, 587 (1978).

6. J. Stöhr, G. Apai, P.S. Wehner, F.R. McFeely, R.S. Williams, and D.A. Shirley, Phys. Rev. B. 14, 5144 (1976).

7. G.A. Burdick, Phys. Rev. 129, 138 (1963).

8. W.J. O'Sullivan, A.C. Switendick, and J.E. Schirber, Phys. Rev. B 1, 1443 (1970).

9. L.F. Wagner, Z. Hussain, and C.S. Fadley, Solid State Commun. 21, 257 (1977).

10. O. Jepsen, D. Glötzel, and A.R. Mackintosh, Phys. Rev. B 23, 2684 (1981).

11. L. Ley, F.R. McFeely, S.P. Kowalczyk, J.G. Jenkin, and D.A. Shirley, Phys. Rev. B. 11, 600 (1975).

12. L. Ley, S.P. Kowalczyk, F.R. McFeely, R.A. Pollak, and D.A. Shirley, Phys. Rev. B 8, 2392 (1973).

13. G.W. Gobeli, F.G. Allen, and E.O. Kane, Phys. Rev. Lett. 12, 94 (1964).

14. H. Becker, E. Dietz, U. Gerhardt, and H. Angermüller, Phys. Rev. B 12, 2084 (1975).

15. J. Hermanson, Solid State Commun. 22, 9 (1977).

16. R.S. Williams, P.S. Wehner, J. Stöhr, and D.A. Shirley, Phys. Rev. Lett. 39, 302 (1977).

17. Z. Hussain, E. Umbach, J.J. Barton, J.G. Tobin, and D.A. Shirley, Phys. Rev. B 25, 672 (1982).

18. Z. Hussain, C.S. Fadley, S. Kono, and L.F. Wagner, Phys. Rev. B 22, 3750 (1980).

19. N.J. Shevchik, Phys. Rev. B 16, 3428 (1977).

20. A.M. Turner, A.W. Donoho, and J.L. Erskine, Phys. Rev. B 29, 2986 (1984). See references therein for previous ARPES studies of Fe.

21. H. Mårtensson and P.O. Nilsson, Phys. Rev. B 30, 3047 (1984), and references therein.

22. S.K. Burke, W.G. Stirling, K.R.A. Ziebeck, and J.G. Booth, Phys. Rev. Lett. 51, 494 (1983).

23. C.R. Fincher, Jr., G. Shirane, and S.A. Werner, Phys. Rev. B 24, 1312 (1981).

24. B.H. Grier, G. Shirane and S.A. Werner, submitted for publication.

25. G. Shirane and W.J. Takei, J. Phys. Soc. Japan Suppl: 17 BIII, 35 (1962).

26. M.K. Wilkinson, E.O. Wollan, W.C. Koehler, and J.W. Cable, Phys. Rev. 127, 2080 (1962).

27. L.M. Corliss, J.M. Hastings, and R.J. Weiss, Phys. Rev. Lett. 3, 211 (1959).

28. A.W. Overhauser, Phys. Rev. 128, 1437 (1962).

29. N.I. Kulikov and E.T. Kulatov, J. Phys. F: Met. Phys. 12, 2291 (1982).

30. H.L. Skriver, J. Phys. F: Met. Phys. 11, 97 (1981).

31. J. Kübler, J. Magn. Magn. Mat. 20, 277 (1980).

32. S. Asano and J. Yamashita, J. Phys. Soc. Jpn. 23, 714 (1967).

33. W.M. Lomer, Proc. Phys. Soc. 80, 489 (1962).

34. L.M. Falicov and M.J. Zuckermann, Phys. Rev. 160, 372 (1967).

35. L.E. Klebanoff, S.W. Robey, G. Liu, and D.A. Shirley, Phys. Rev. B 30, 1048 (1984).

36. D.R. Grempel, Phys. Rev. B 24, 3928 (1981).

37. G. Allan, Surface Science Reports 1, 121 (1981).

38. G. Allan, Phys. Rev. B 19, 4774 (1979).

39. G. Allan, Surf. Sci. 74, 79 (1978).

40. L.I. Johansson, L.-G. Petersson, K.-F. Berggren, and J.W. Allen, Phys. Rev. B 22, 3294 (1980).

41. G. Gewinner, J.C. Peruchetti, A. Jaéglé, and R. Pinchaux, Phys. Rev. B 27, 3358 (1983).

42. D. Aitelhabti, G. Gewinner, J.C. Peruchetti, R. Riedinger, D. Spanjaard, and G. Tréglia, J. Phys. F: Met. Phys. 14 1317 (1984).

43. S.D. Kevan and D.A. Shirley, Phys. Rev. B 22, 542 (1980).

44. J.S. Foord and R.M. Lambert, Surf. Sci. 115, 141 (1982).

45. A.G. Baca, L.E. Klebanoff, M.A. Schulz, E. Paparazzo and D.A. Shirley, to be published.

46. W.C. Koehler, R.M. Moon, A.L. Trego, and A.R. Mackintosh, Phys. Rev. 151, 405 (1966).

47. Y. Hamaguchi, E.O. Wollan, and W.C. Koehler, Phys. Rev. 138, 737 (1965).

48. G.D. Mahan, Phys. Rev. B 2, 4334 (1970).

49. T.-C. Chiang, J.A. Knapp, M. Aono, and D.E. Eastman, Phys. Rev. B 21, 3513 (1980).

50. P.J. Feibelman and D.E. Eastman, Phys. Rev B 10, 4932 (1974).

51. C.J. Powell, Surf. Sci. 44, 29 (1974).

52. A.J. Holden, V. Heine, and J.H. Samson, J. Phys. F: Met. Phys. 14, 1005 (1984).

53. D.I. Bolef and J. De Klerk, Phys. Rev. 129, 1063 (1963).

54. S.N. Evangelou, H. Hasegawa, and D.M. Edwards, J. Phys. F: Met. Phys. 12, 2035 (1982).

55. H. Hasegawa, J. Phys. F: Met. Phys. 14, 1235 (1984).

56. Y. Takahashi and T. Moriya, J. Phys. Soc. Jpn. 52, 4342 (1983).

57. V. Heine, J. Phys. F: Met. Phys. 11, 2645 (1981).

58. A. Ziegler, Phys. Rev. Lett. 48, 695 (1982).

59. D.M. Edwards, J. Phys. F: Met. Phys. 12, 1789 (1982).

60. H. Hasegawa, J. Phys. Soc. Jpn. 49, 963 (1980).

61. J.L. Morán-López, K.H. Bennemann, and M. Avignon, Phys. Rev. B 23, 5978 (1981).

62. J. Hubbard, Phys. Rev. B 23, 5974 (1981).

63. H. Hasegawa, J. Phys. Soc. Jpn. 49, 178 (1980).

64. M.V. You, V. Heine, A.J. Holden, and P.J. Lin-Chung, Phys. Rev. Lett 44, 1282 (1980).

65. J. Hubbard, Phys. Rev. B 19, 2626 (1979).

66. H. Hasegawa, J. Phys. Soc. Jpn. 46, 1504 (1979).

67. V. Korenman, J.L. Murray, and R.E. Prange, Phys. Rev. B 16, 4032 (1977).

68. V. Korenman, J.L. Murray, and R.E. Prange, Phys. Rev. B 16, 4048 (1977).

69. J.B. Sokoloff, J. Phys. F: Met. Phys. 5, 1946 (1975).

70. H. Capellmann, J. Phys. F: Met. Phys. 4, 1466 (1974).

71. An ARPES investigation of ordered metal overlayers has shown that three-dimensional band properties require ~ 15 Å to develop.: J.G. Tobin, S.W. Robey, L.E. Klebanoff, and D.A. Shirley, Phys. Rev. B 28, 6169 (1983).

72. P.L. Wincott, N.B. Brookes, D.S. Law, and G. Thornton, Vacuum 33, 815 (1983).

FIGURE CAPTIONS

FIG. 1. The real space spin-lattice of commensurate antiferromagnetic chromium. The topmost atoms define the (001) crystal plane.

FIG. 2. The AF (solid line) and PM (dashed line) Brillouin zones in the (100) mirror plane (defined by the [001] and [010] vectors). High symmetry points in the AF Brillouin zone are labelled with the conventional greek letters; those in the PM Brillouin zone are labelled with the appropriate letters enclosed by parentheses.

FIG. 3. (a): The dispersion of a model sinusoidal band along the [010] direction for a PM state. (b): The dispersion of the sinusoidal bands along the [010] direction for a commensurate AF state. (c): A first-order estimate of the [010] dispersion of sinusoidal bands when an incommensurate SDW exists along the [010] direction. The deviation from commensurate periodicity, δ, is assigned the value 0.03 Å^{-1} that is observed near room temperature (Ref. 23). The symmetry point notation is that adopted in Fig. 2.

FIG. 4. The experimental geometry. The [001] direction lies normal to the Cr(001) surface. The polar angle of electron detection θ_e (degrees) was varied in the (100) mirror plane. For our synchrotron radiation ARPES

measurements, the vector potential $\underset{\sim}{A}$ lies in the (100) mirror plane and makes a 25.0° angle with the surface normal, as shown. We label this geometry P-polarization. For our measurements using HeI_α radiation, the $\underset{\sim}{A}$ vector could also be oriented along the [100] direction perpendicular to the (100) mirror plane (S-polarization).

FIG. 5. (a): Wavevector conservation (eqn. (1) in text) depicted in the PM Brillouin zone of Fig. 2. The solid line is the final-state symmetry line that is used to probe the [010] electronic structure (see text). (b): Wavevector conservation viewed in the AF Brillouin zone of Fig. 2. The square around $\underset{\sim}{k}^f$ in 5(b) has dimensions (0.24 $Å^{-1}$ x 0.24 $Å^{-1}$) and gives the k-space resolution in the (100) plane for the UPS spectra. The dashed line is the final-state symmetry line that is used to probe the [010] electronic structure (see text). The symmetry notation used in both 5(a) and 5(b) is that adopted in Fig. 2.

FIG. 6. UPS specta of Cr(001) at 298 K. The photon energy $h\nu$ (eV) and the polar angle of electron detection θ_e (degrees) are listed for each spectrum. The values $k_{\|}^f$ ($Å^{-1}$) are the components of the final-state wavevectors parallel to the surface for the peaks labelled with a tic mark. The intensities of the spectra have been scaled to clarify the presentation.

FIG. 7. Experimentally observed band dispersions along the [010] symmetry line. Values of E_{IN} (eV) are plotted versus $k_{\|}^{f}$ ($\AA^{-1}$) for the features observed in our UPS spectra. The size of the symbol gives the experimental error in E_{IN}. The greek letters at the top of the figure label the [010] symmetry line in the manner appropriate for simple cubic symmetry. The solid lines are the Γ-X-Γ band dispersions for commensurate AF chromium as calculated by Skriver (Ref. 30). Arabic numerals label the symmetry of these theoretical bands. A peak is observed at $E_{IN} \sim 0.25$ eV for many values of $k_{\|}^{f}$. A feature is also present for $k_{\|}^{f} < 0.3$ $\AA^{-1}$ with $0.7 \leq E_{IN} \leq 0.9$ eV. Both have been previously assigned (Ref. 35) to the ferromagnetic surface electronic structure and are omitted from this figure for clarity.

FIG. 8. The onset of Band III at $E_{IN} \sim 0.9$ eV. The value $k_{\|}^{f}$ ($\AA^{-1}$) is given for the Band III spectral peak. All spectral intensities have been scaled for presentation.

FIG. 9. A comparison of Cr(001) UPS spectra before (line) and after (dots) 1L CO exposure. The experimental geometry is that of Fig. 4; $h\nu = 21.22$ eV, $\theta_e = 40.6^{\circ}$. The contamination-induced peak at $E_{IN} = 6.7$ eV is assigned to impurity (carbon and oxygen) 2p photoemission. The intensities of the two spectra have been normalized at $E_{IN} = 8.0$ eV.

FIG. 10. UPS spectra displaying the persistence of Band I and Band II splitting (dashed line) near Γ. The electron detection angle θ_e is given for each spectrum. The value $k_{\|}$ is listed for the Band I and Band II peaks (they have nearly the same values of $k_{\|}$). Spectral intensities have been scaled to clarify the presentation.

FIG. 11. Normal-emission ($\theta_e = 0^\circ$) SXPS spectra for Cr(001). The values $k_\perp$ ($\AA^{-1}$) are the wavevector magnitudes (along [001]) of the initial states responsible for the peaks labelled with a tic mark. These $k_\perp$ values have been calculated using $V_o = 10.8$ eV. Spectra have been scaled for presentation.

FIG. 12. Line: Normal-emission SXPS spectrum of Cr(001) using $h\nu$ = 130.0 eV. Dots: Normal-emission SXPS spectrum of Cr(001) using $h\nu$ = 80.0 eV. The $k_\perp$ values are the magnitudes of the wavevectors (along [001]) of the initial states producing the near-surface photoelectron peaks at E_{IN} ~ 3.5 eV. The two spectra have been normalized at E_{IN} = 6.5 eV.

FIG. 13. Experimentally observed band dispersions along [001]. Values of E_{IN} (eV) are plotted versus $k_\perp$ ($\AA^{-1}$) for the near-surface features observed in our SXPS spectra. Features observed with $E_{IN} < 1$ eV have been previously assigned (Ref. 35) to the ferromagnetic surface electronic structure, and are omitted from this figure. The size of

the symbol gives the error in determining E_{IN} for the near-surface features. For clarity, the initial-state $k_\perp$ values have been recalculated using V_o = 16.6 eV (see text). The solid lines are Skriver's theoretical Γ-X-Γ band dispersions for commensurate AF chromium (Ref. 30). Arabic numerals label the symmetry of these calculated bands. The [001] symmetry line is labelled at the top of the figure using the simple cubic symmetry notation.

FIG. 14. The polarization dependence of Band I features. Spectrum (a): Normal-emission ($\theta_e = 0^\circ$) spectrum of Cr(001) using $h\nu$ = 21.22 eV. The $\underset{\sim}{A}$ vector is oriented as shown in Fig. 4 (P-polarization). Spectrum (b): Same as (a) only with the $\underset{\sim}{A}$ vector oriented in the surface plane along the [100] direction (perpendicular to the (100) mirror plane). This is S-polarization. Spectrum (c): UPS spectrum taken in P-polarization; $\theta_e = 40.6^\circ$, $h\nu$ = 21.22 eV. Spectrum (d): same as (c) only with S-polarization. The spectral intensities have been scaled.

FIG. 15. The influence of temperature on Band I. The value $k_\parallel$ is given for the Band I spectral peak at E_{IN} = 3.32(5) eV. The temperature range is listed for each spectrum. The intensities have been scaled for presentation.

FIG. 16. The influence of temperature on Band I. The value $k_\parallel$ is given for the Band I peak at E_{IN} = 3.07(5) eV. All intensities have been scaled.

FIG. 17. The theoretical prediction for Cr(001) surface and near-surface magnetism. Atoms whose magnetic moments point to the right are indicated by darkened spheres. Atoms whose magnetic moments point to the left are symbolized by open spheres. The diameter of the sphere representing an atom at layer l is drawn proportional to the magnitude of the atom's magnetic moment M(l) as predicted by eqn. (10) in the text.

FIG. 18. Left scale: The temperature dependence of the binding energy E_{IN} of the surface feature 2. Right scale: The temperature dependence of the Band I spectral intensity, normalized to the value observed at 298 K. The dashed line is only a guide for the eye.

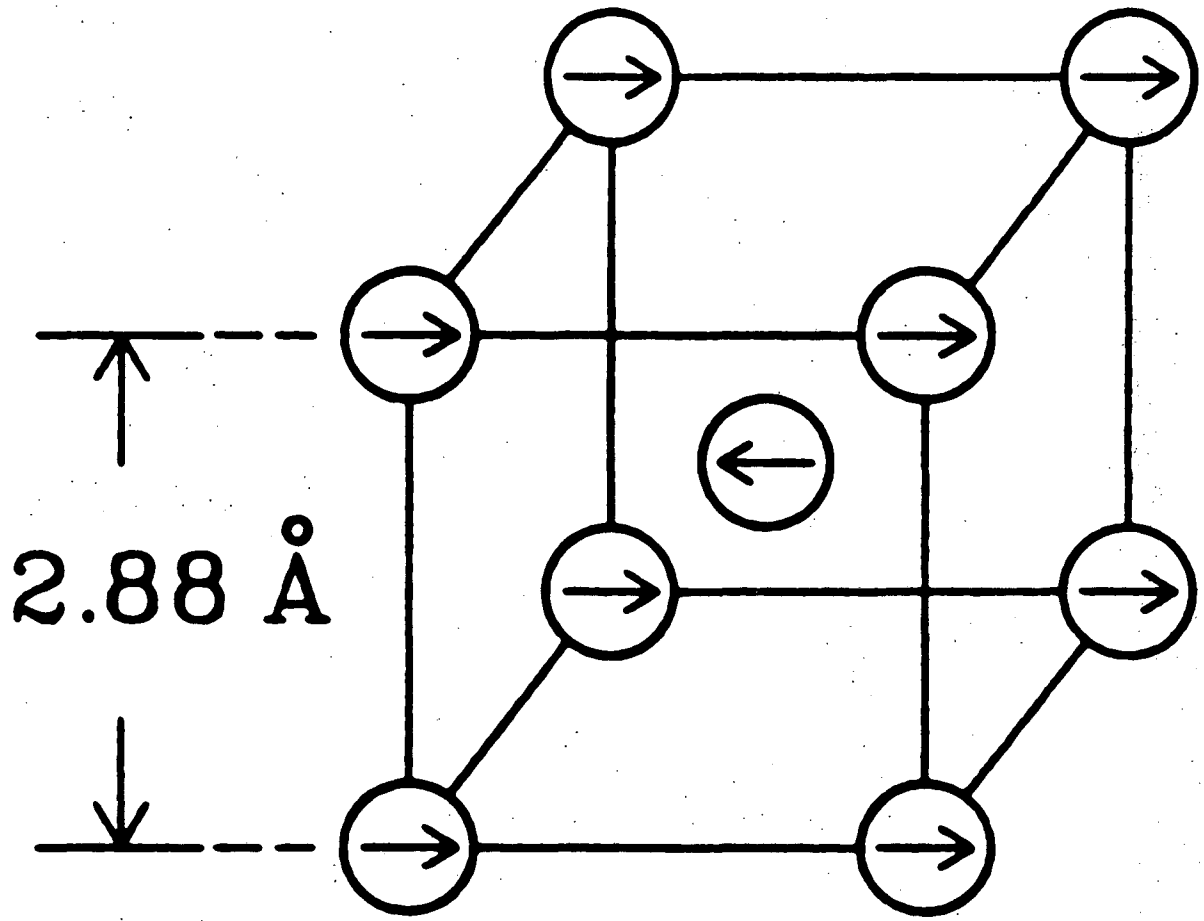

XBL 8412-5100

Figure 1

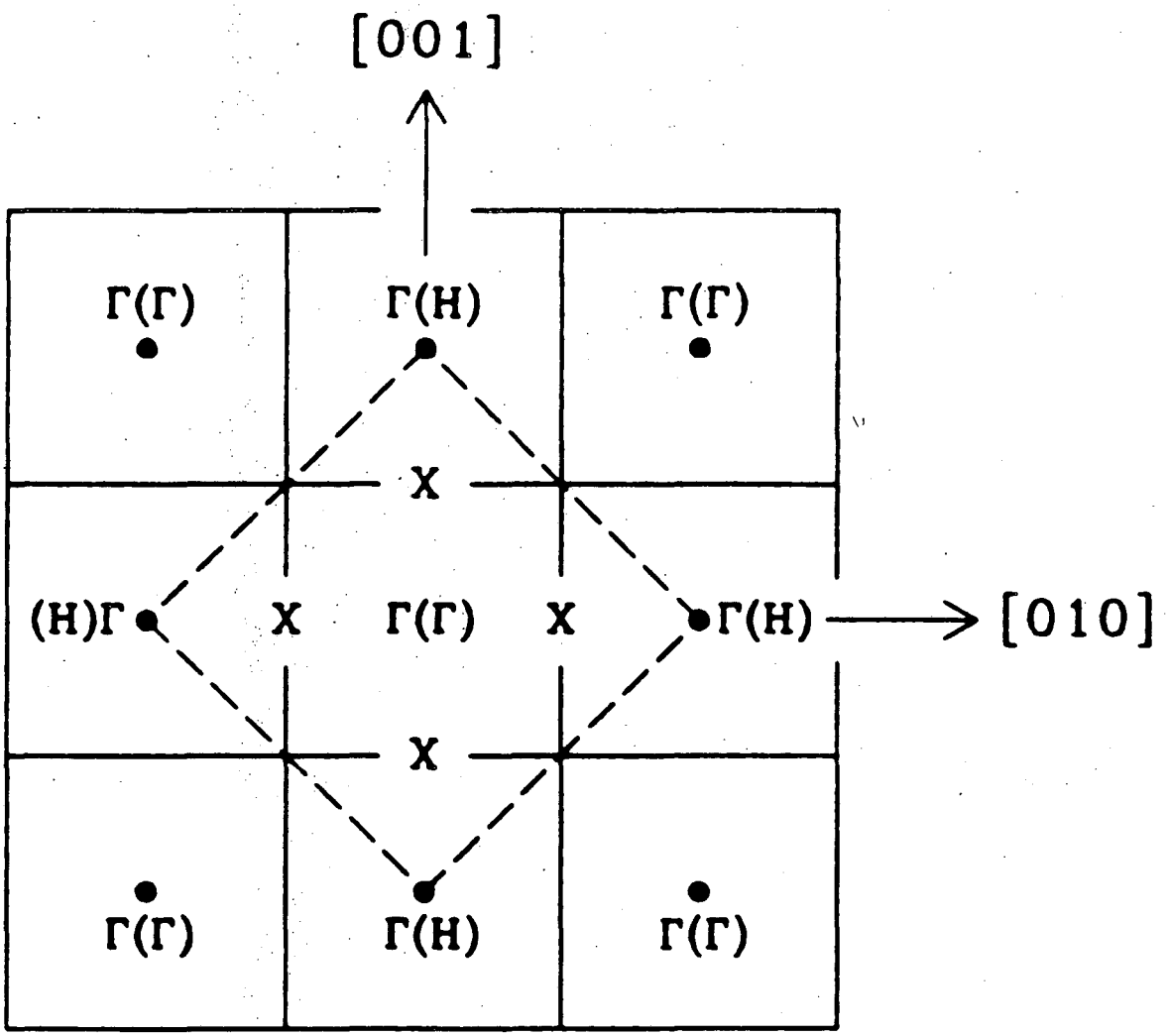

XBL 8412-5411

Figure 2

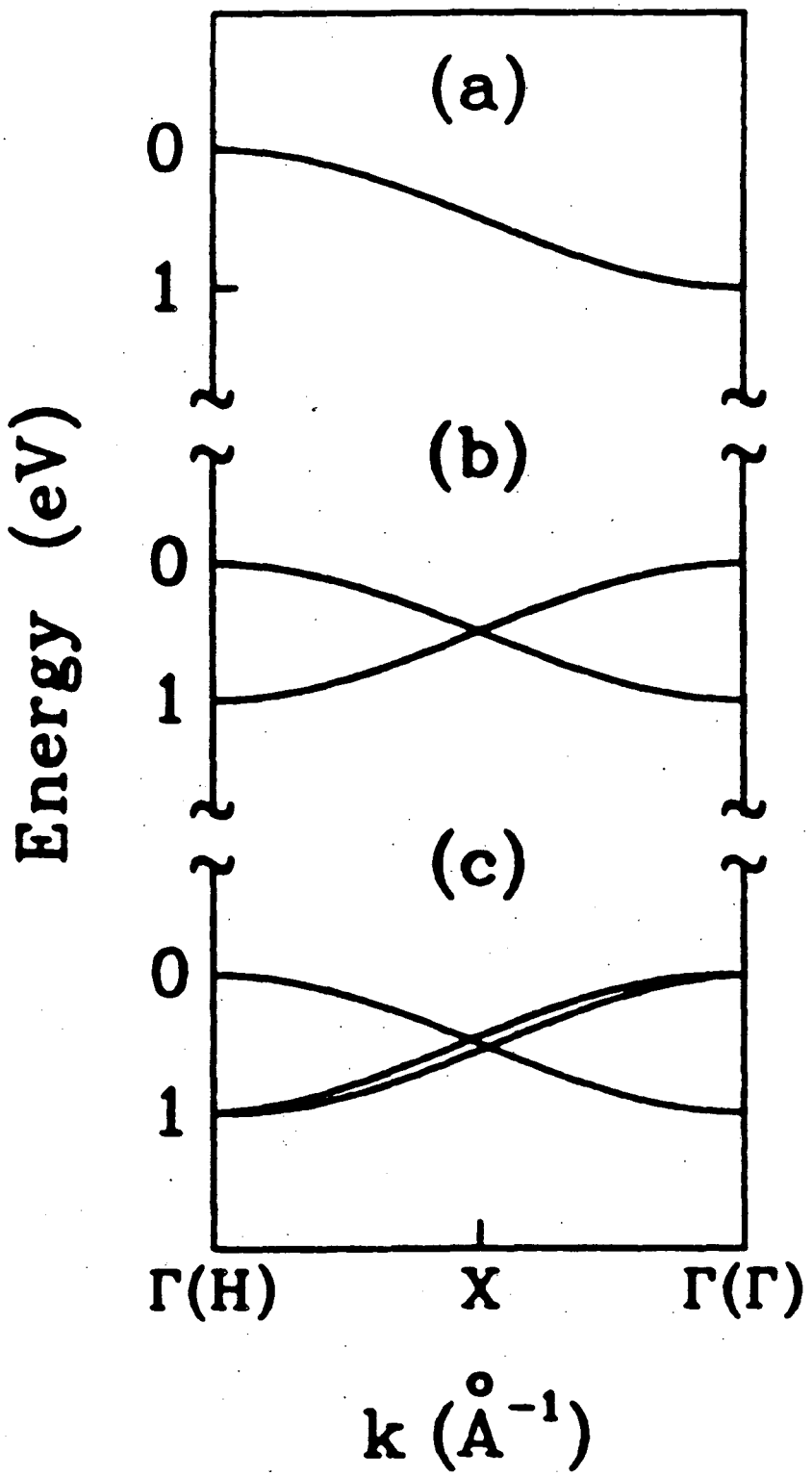

XBL 8412-5101

Figure 3

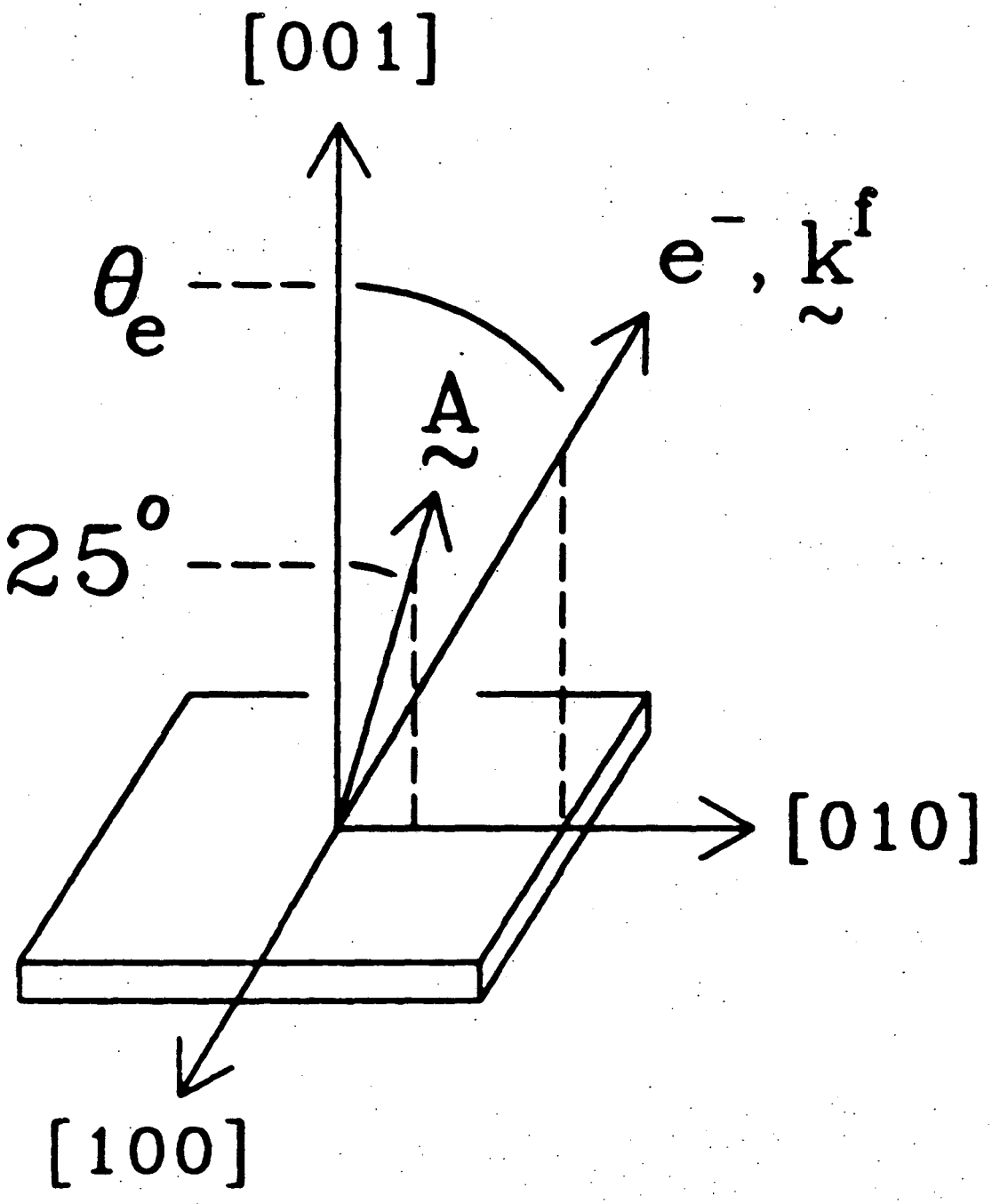

XBL 8412-5408

Figure 4

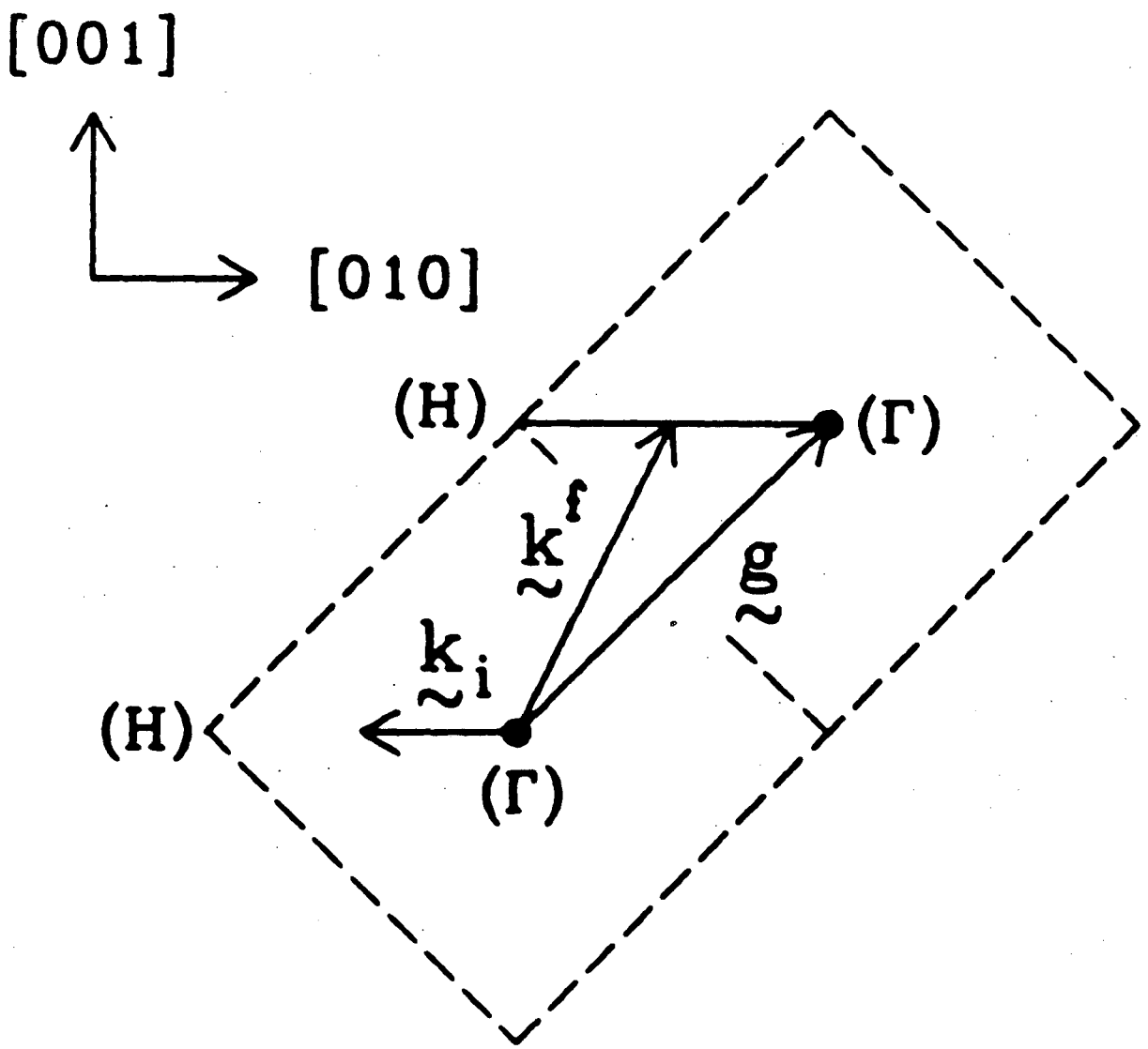

XBL 8412-5410

Figure 5(a)

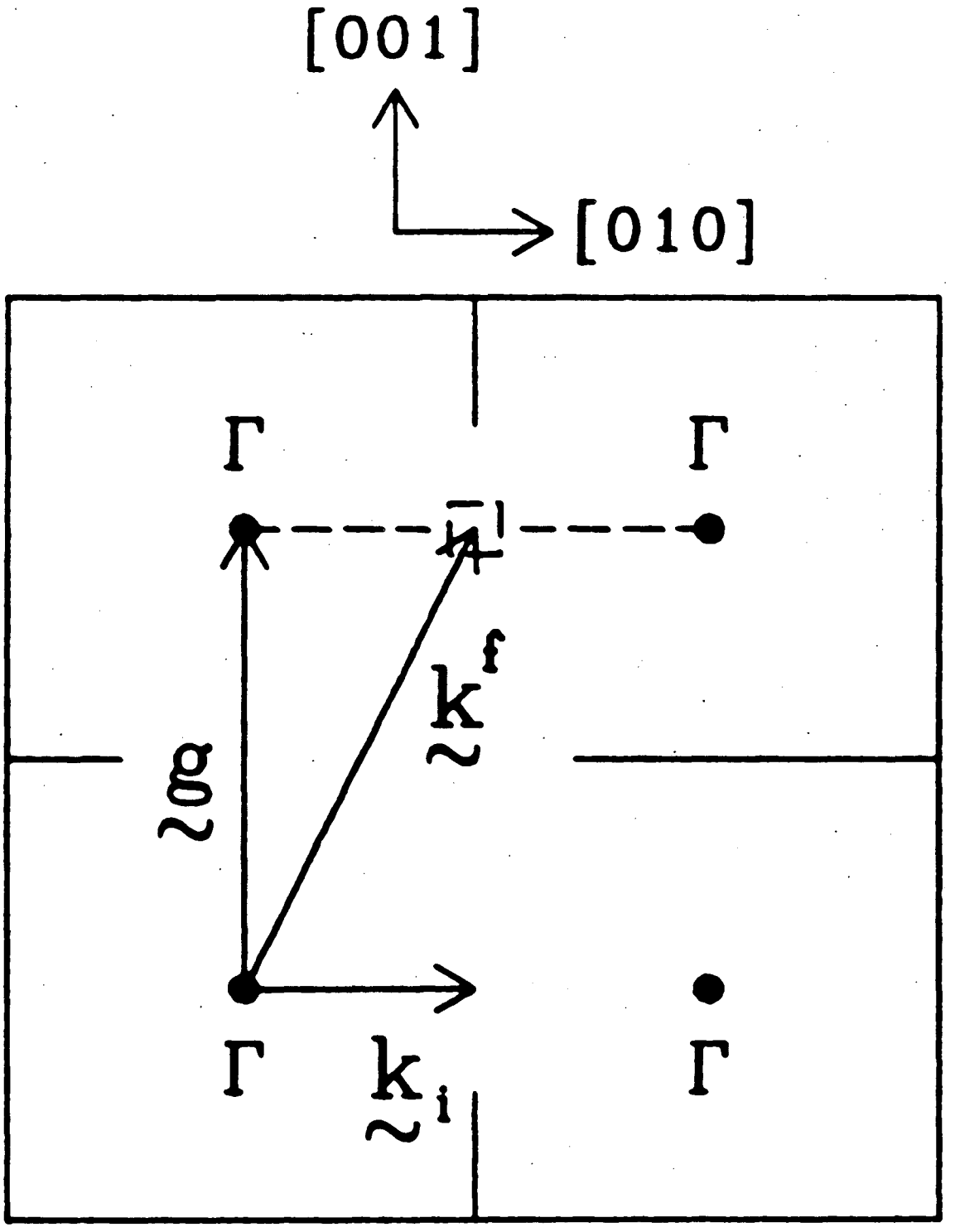

XBL 8412-5409

Figure 5(b)

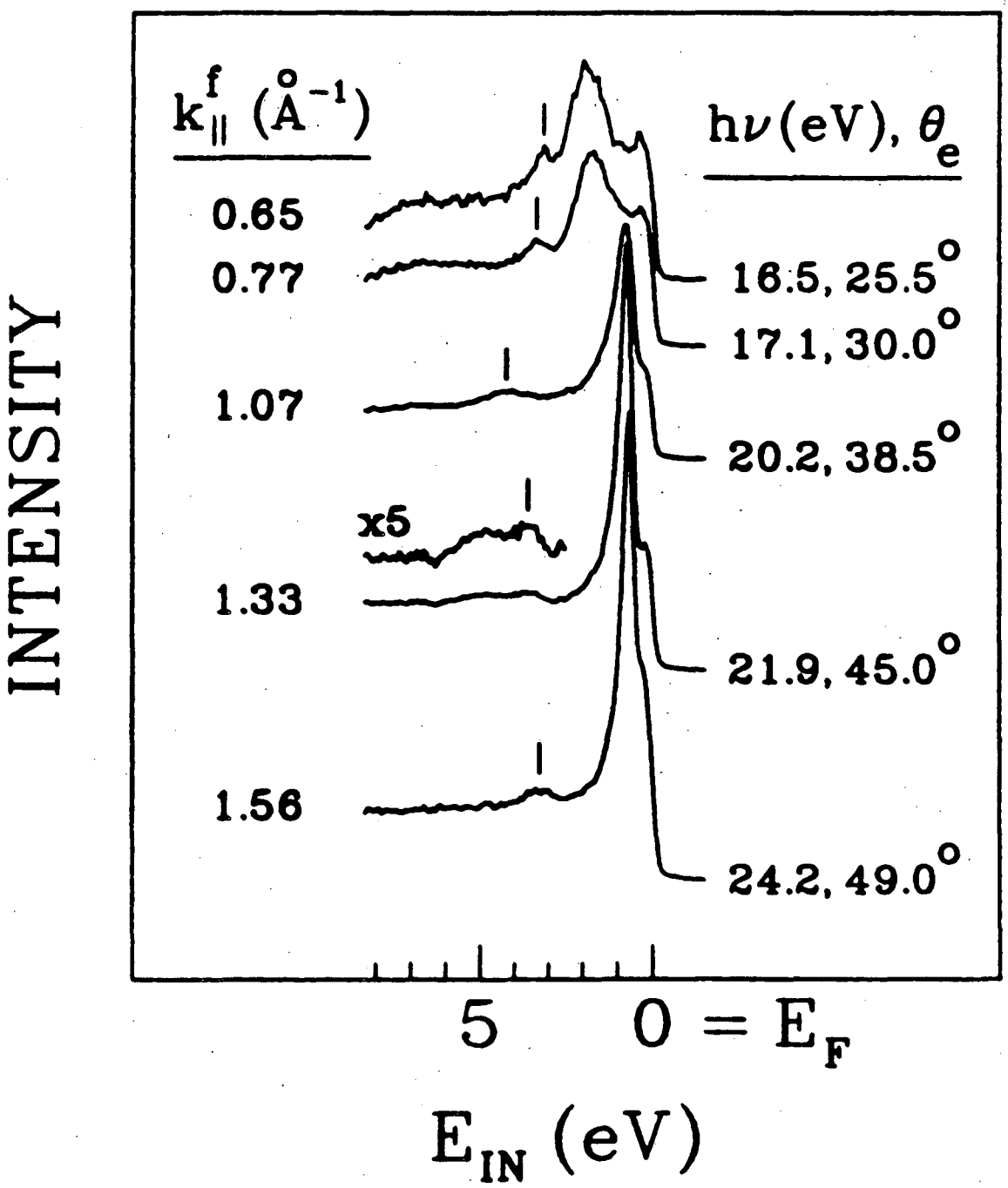

XBL 8412-5114

Figure 6

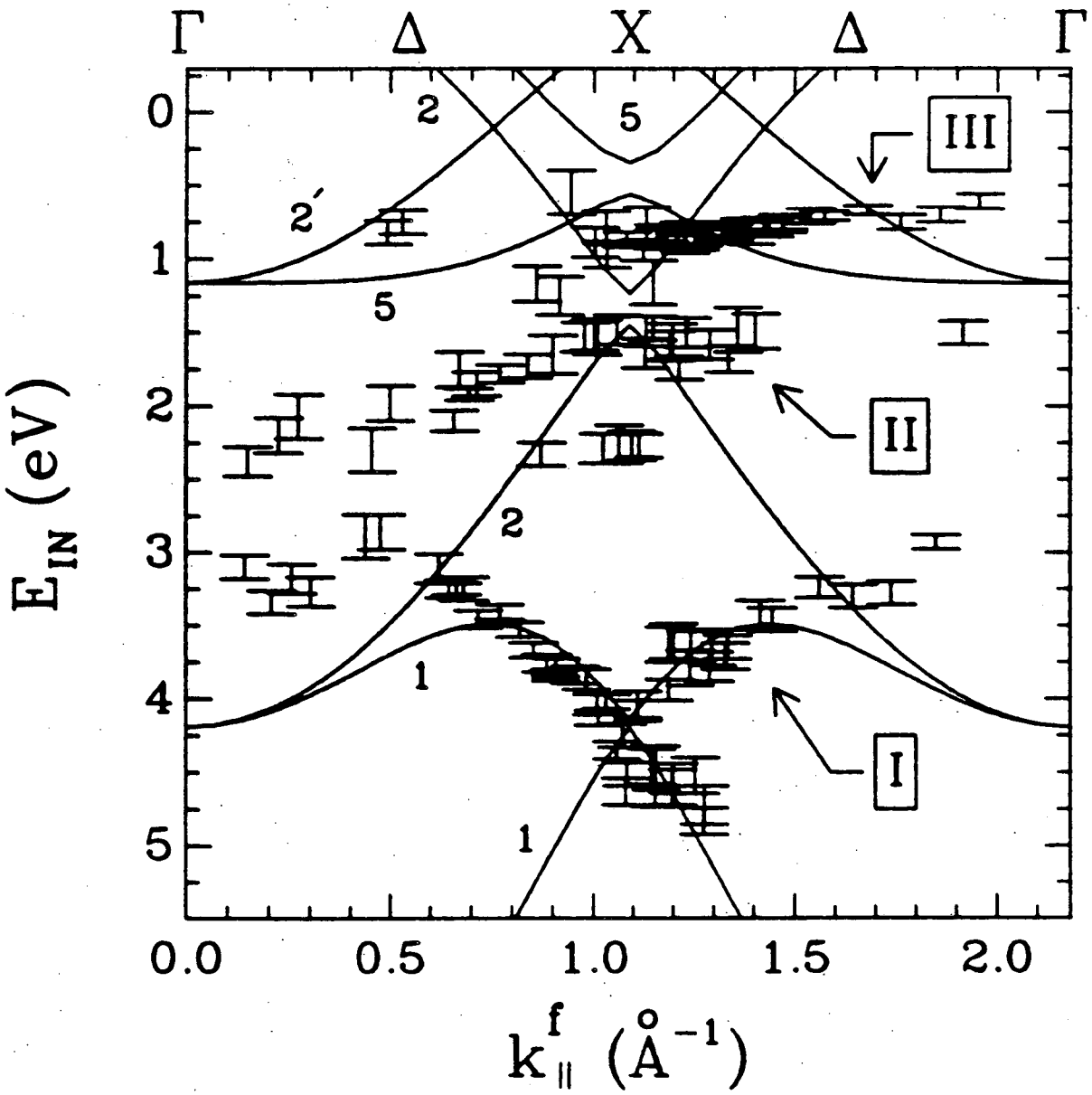

XBL 8412-5113

Figure 7

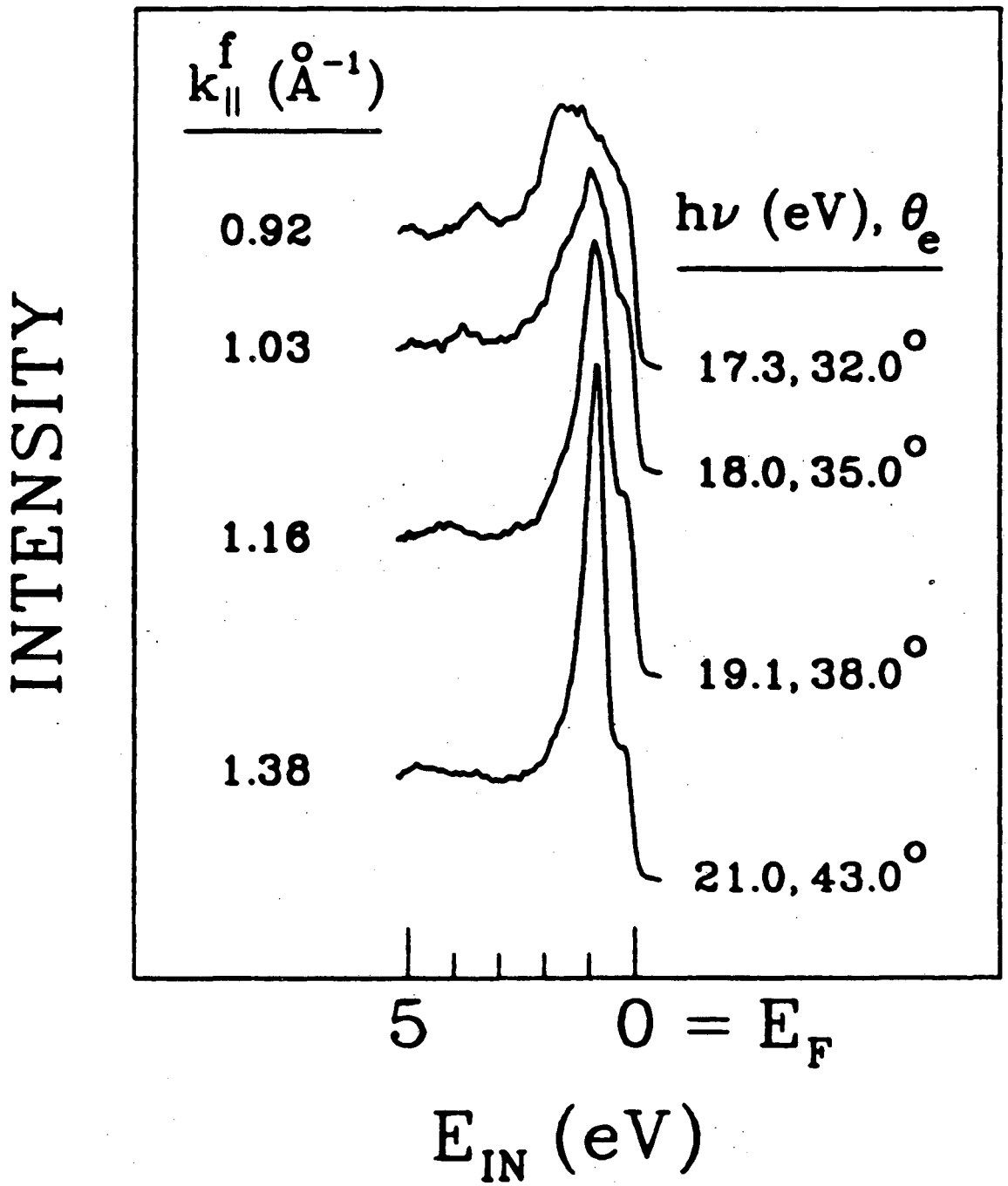

XBL 8412-5112

Figure 8

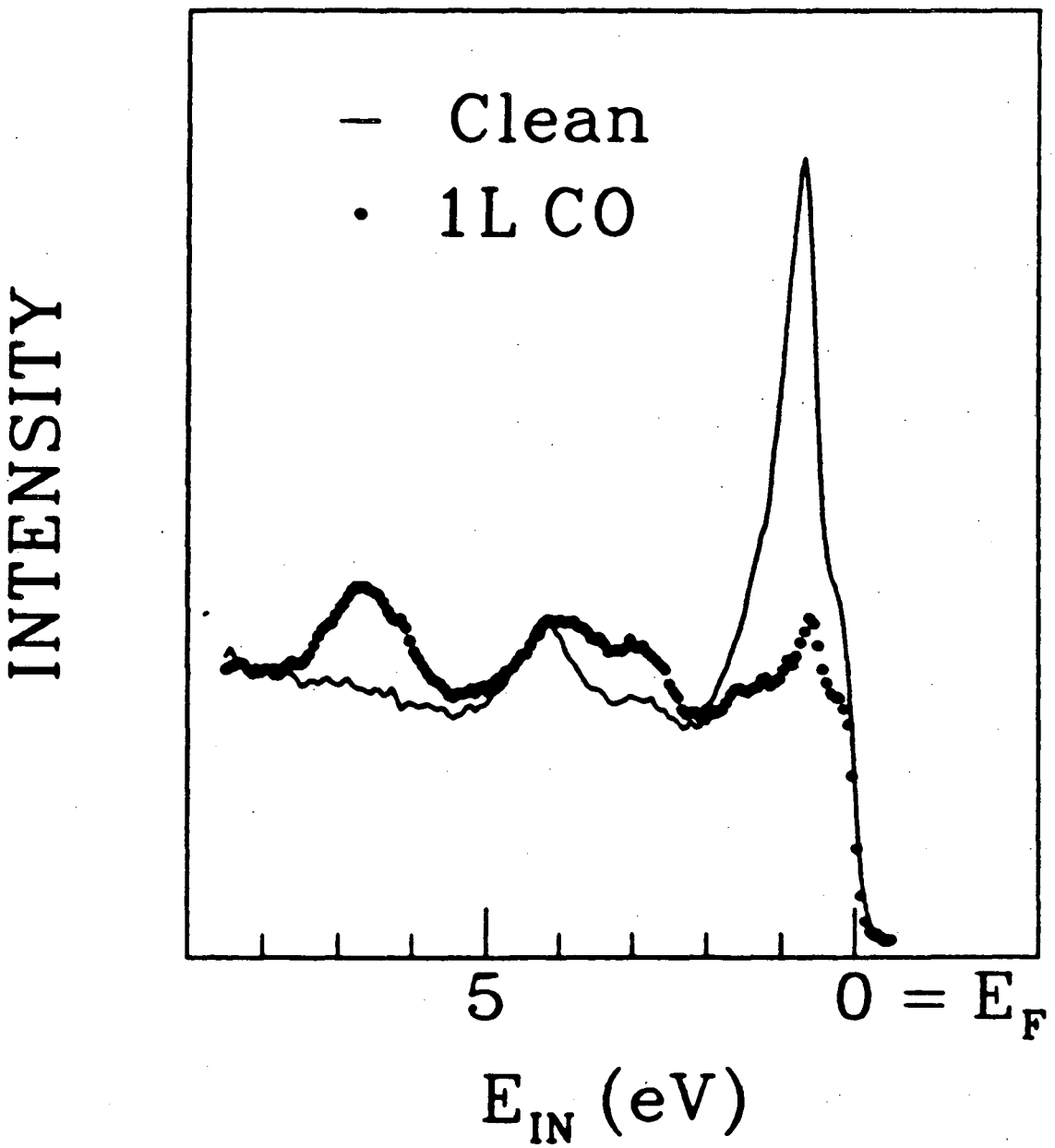

XBL 8412-5111

Figure 9

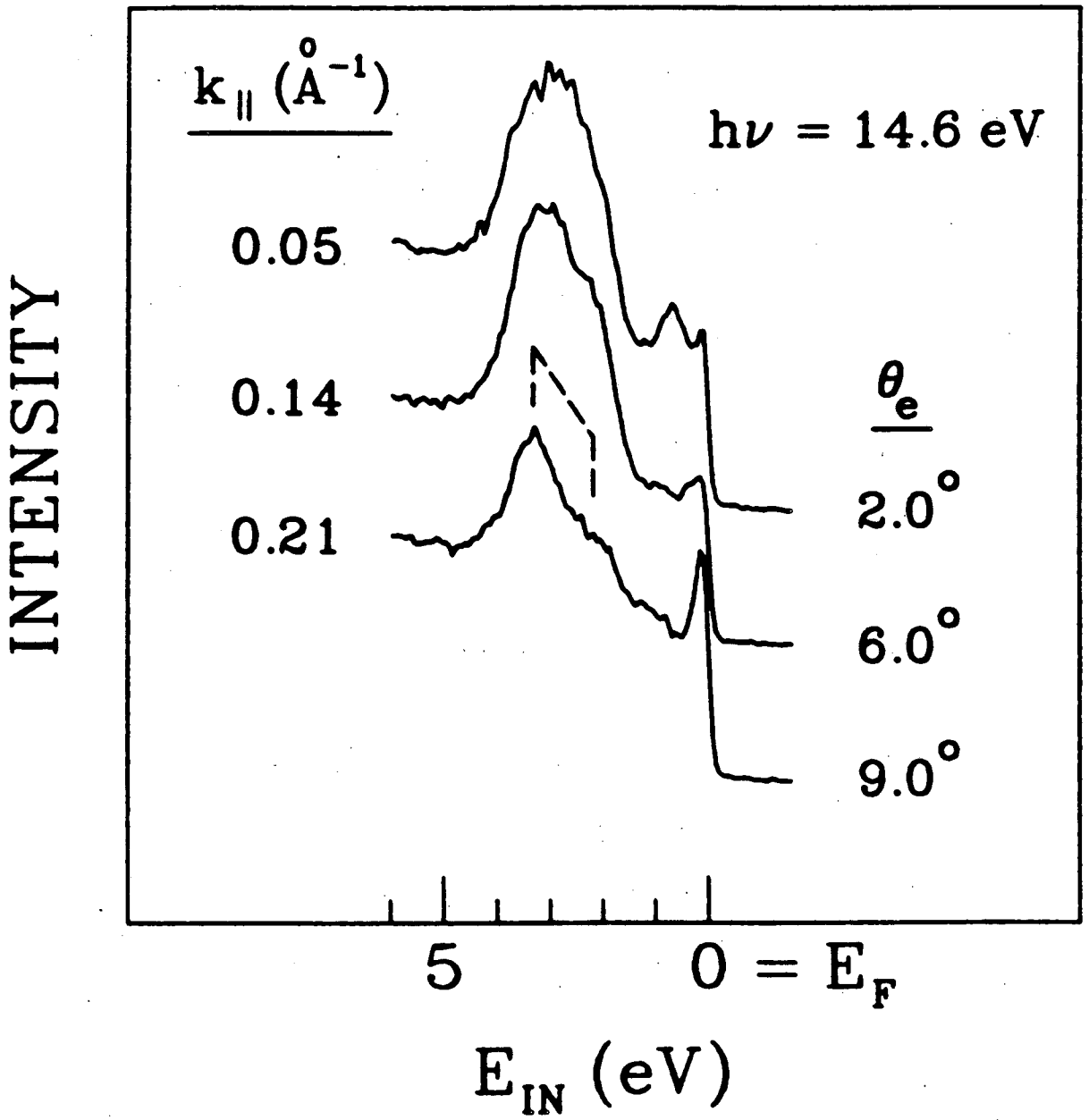

XBL 8412-5110

Figure 10

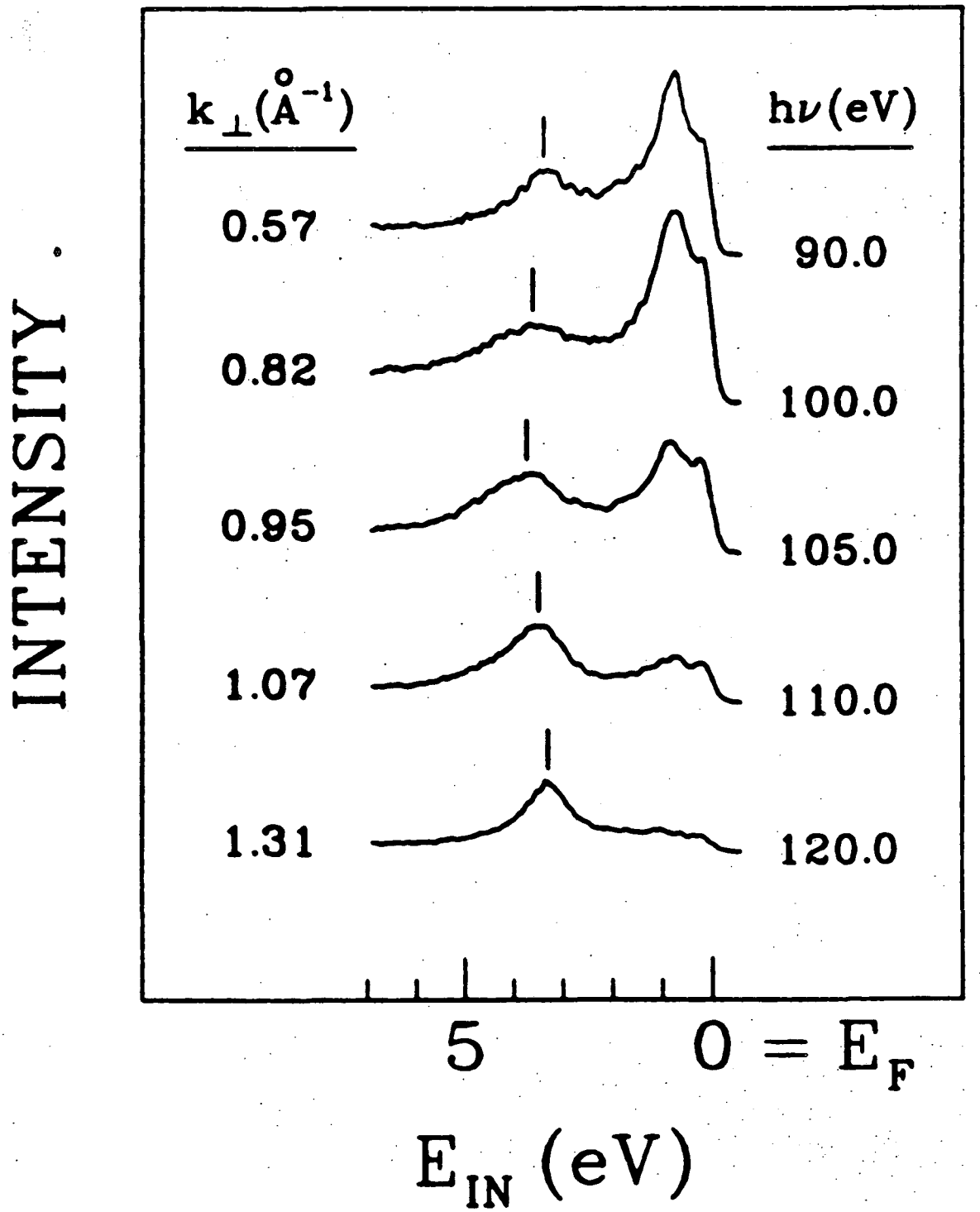

XBL 8412-5109

Figure 11

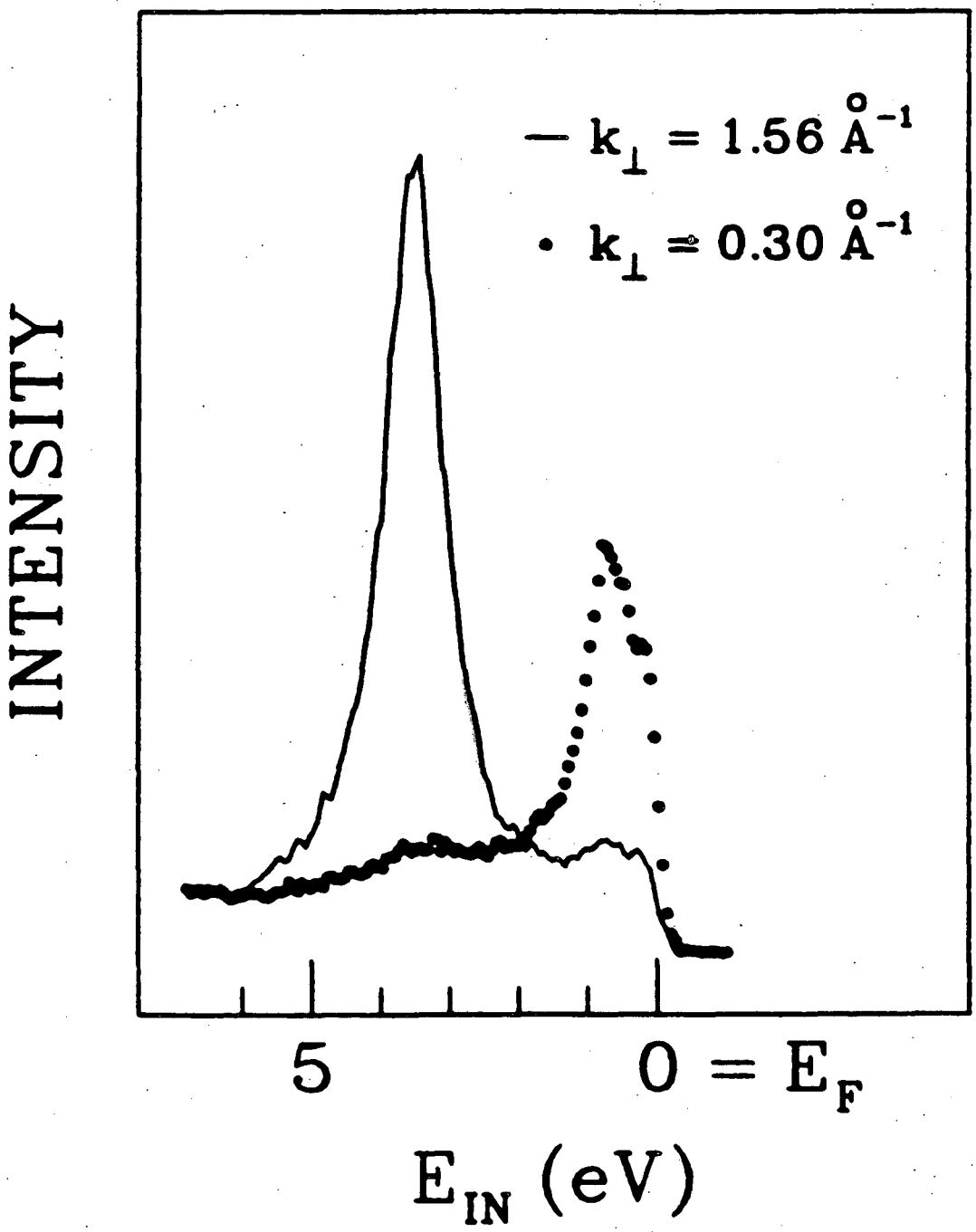

XBL 8412-5107

Figure 12

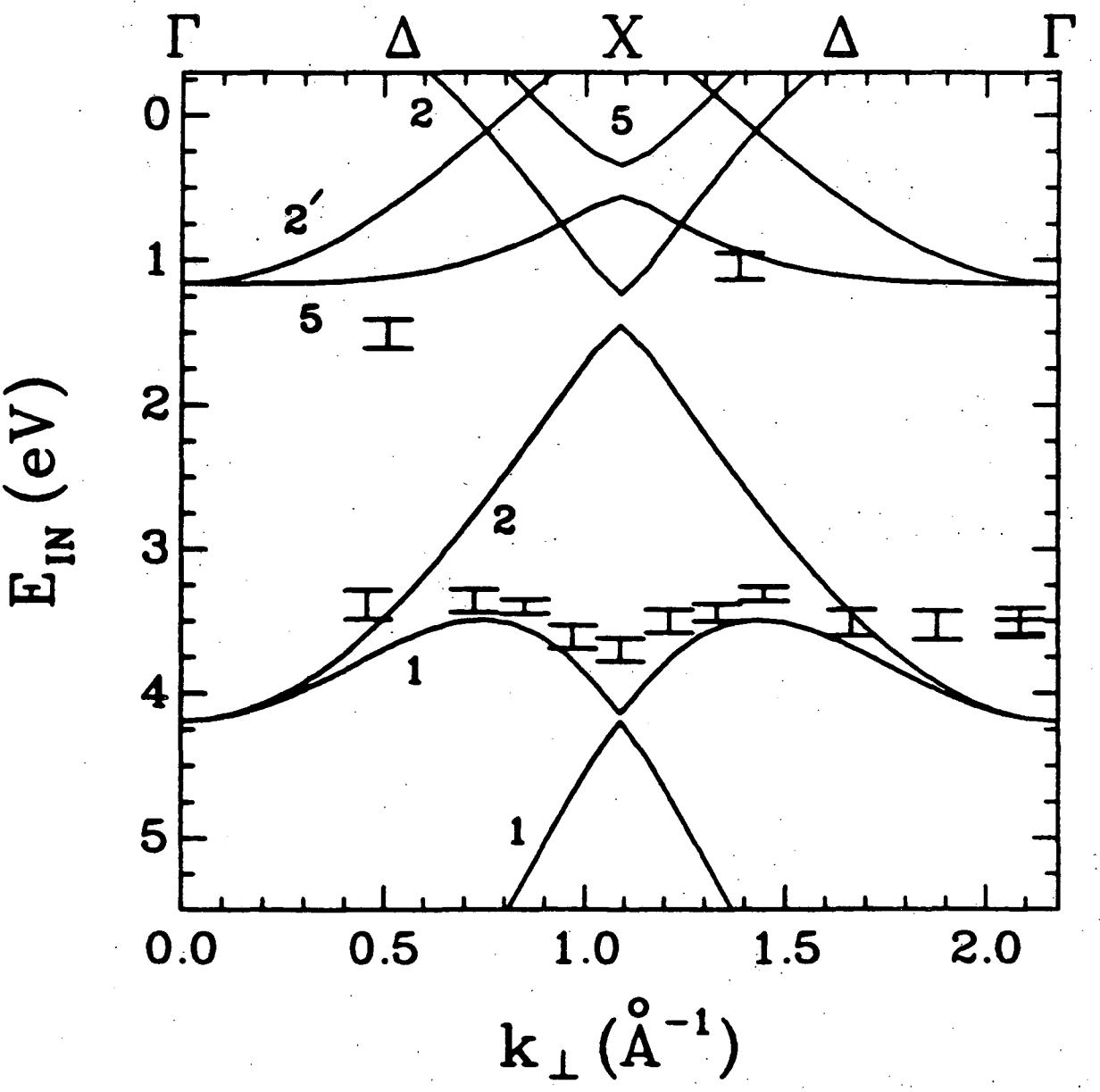

XBL 8412-5108

Figure 13

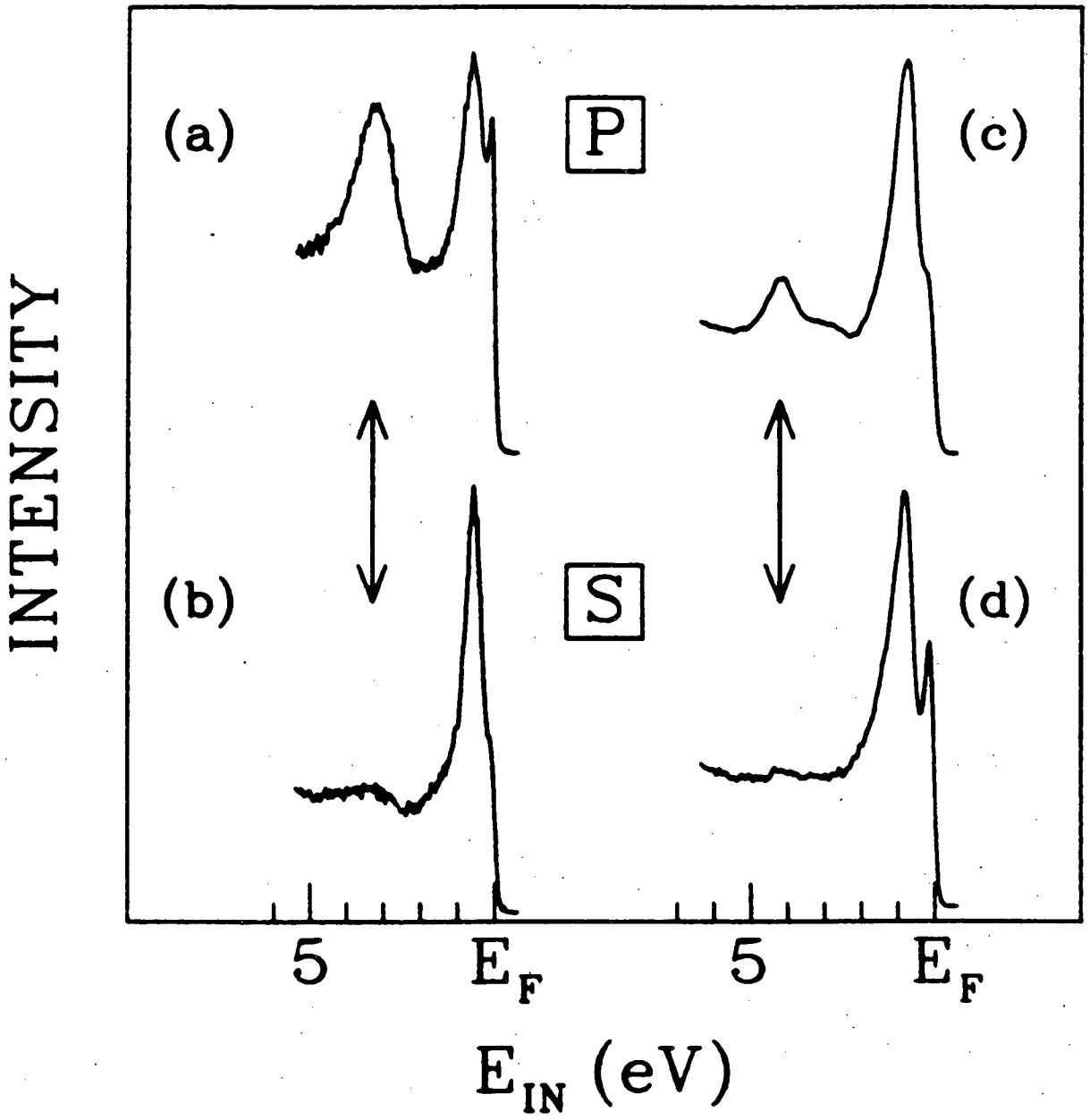

XBL 8412-5106

Figure 14

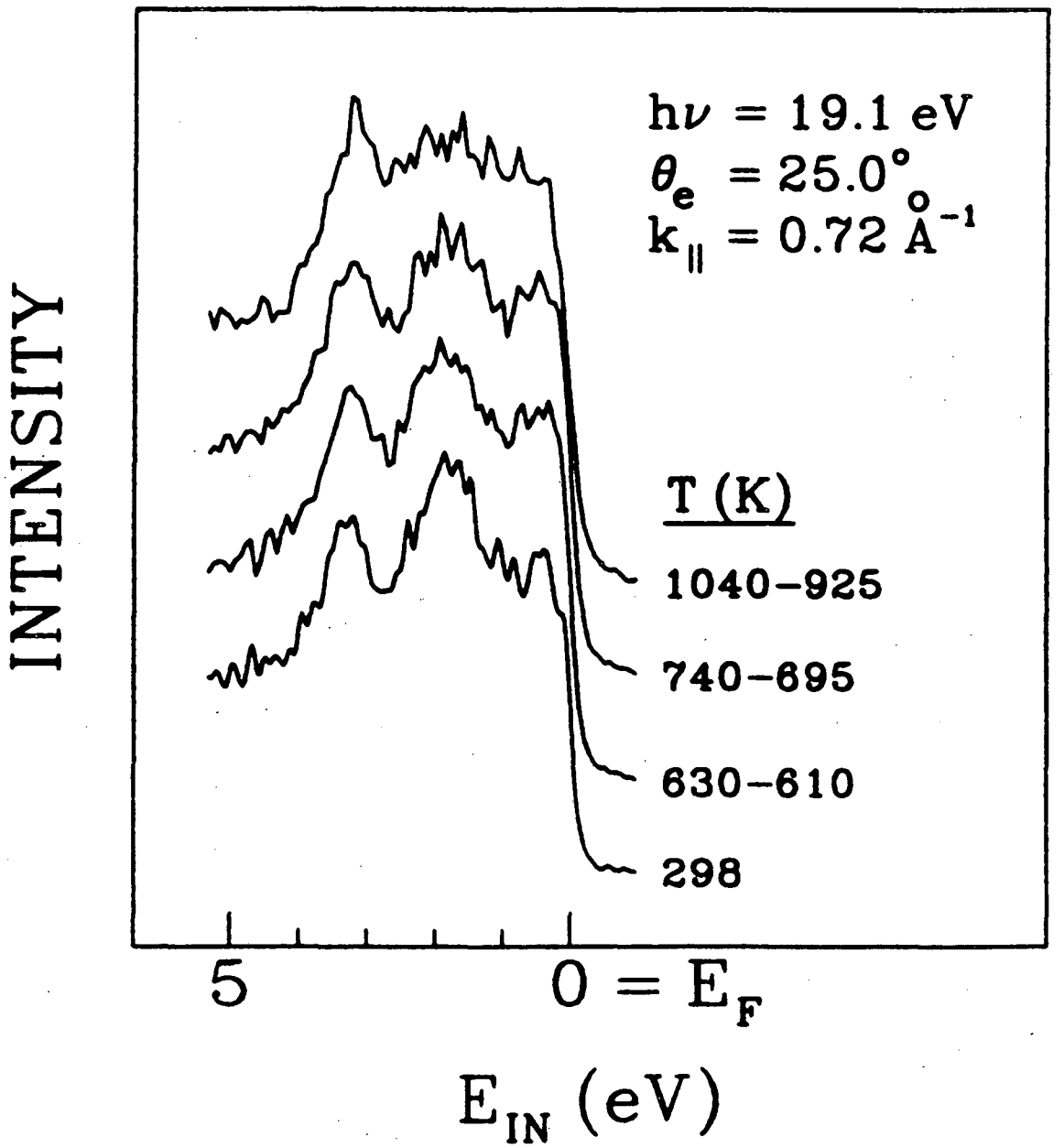

XBL 8412-5105

Figure 15

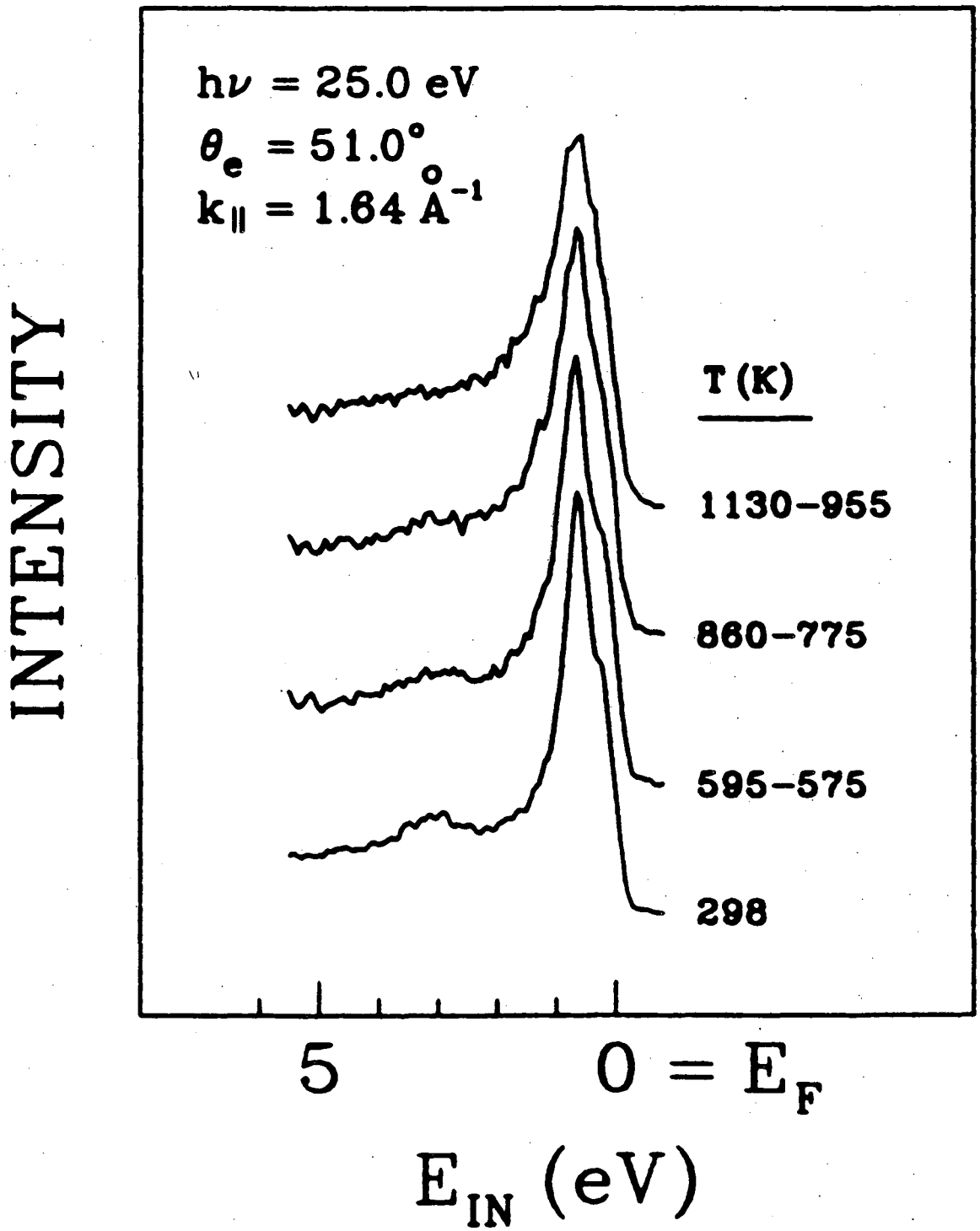

XBL 8412-5104

Figure 16

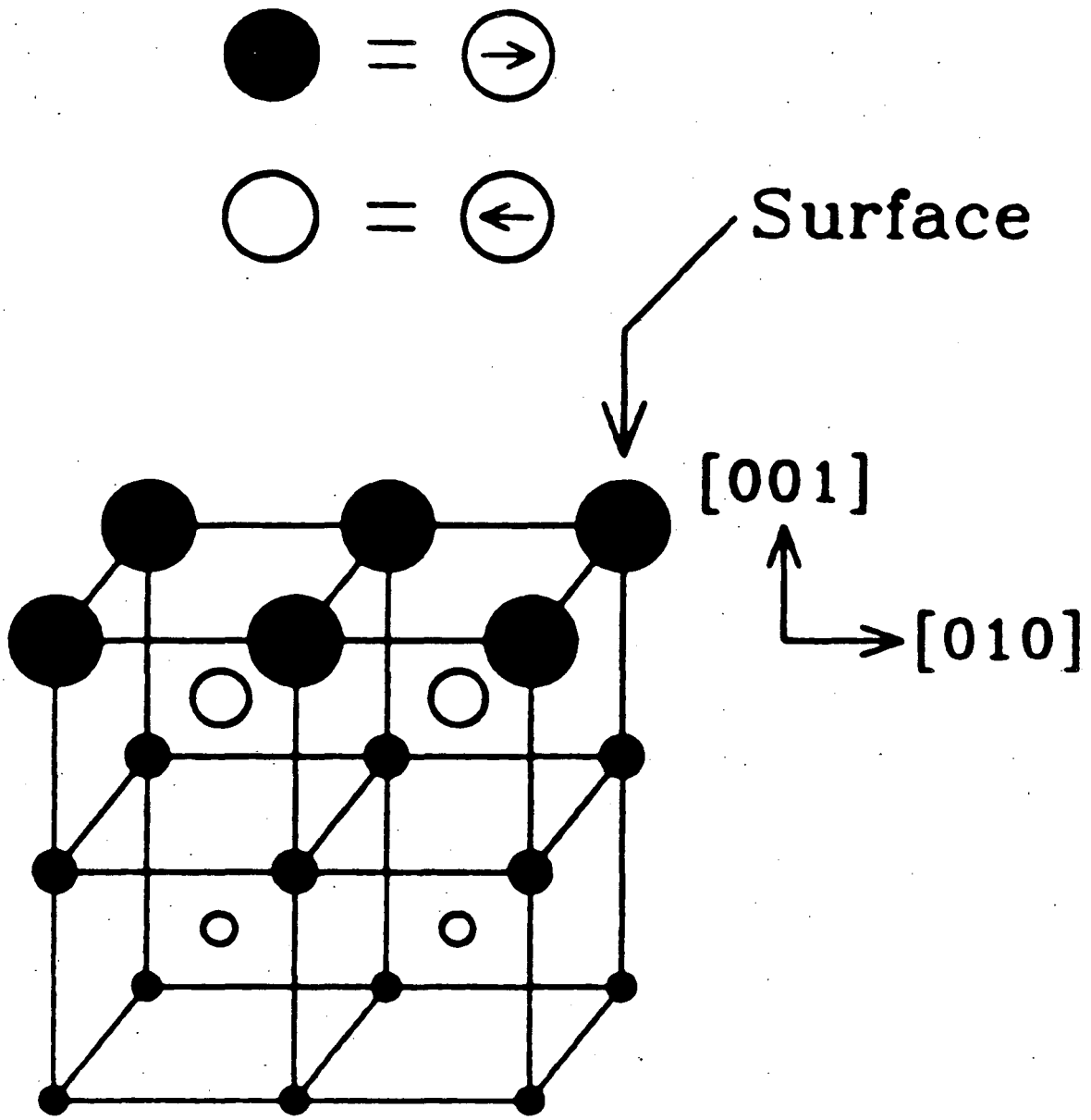

XBL 8412-5407

Figure 17

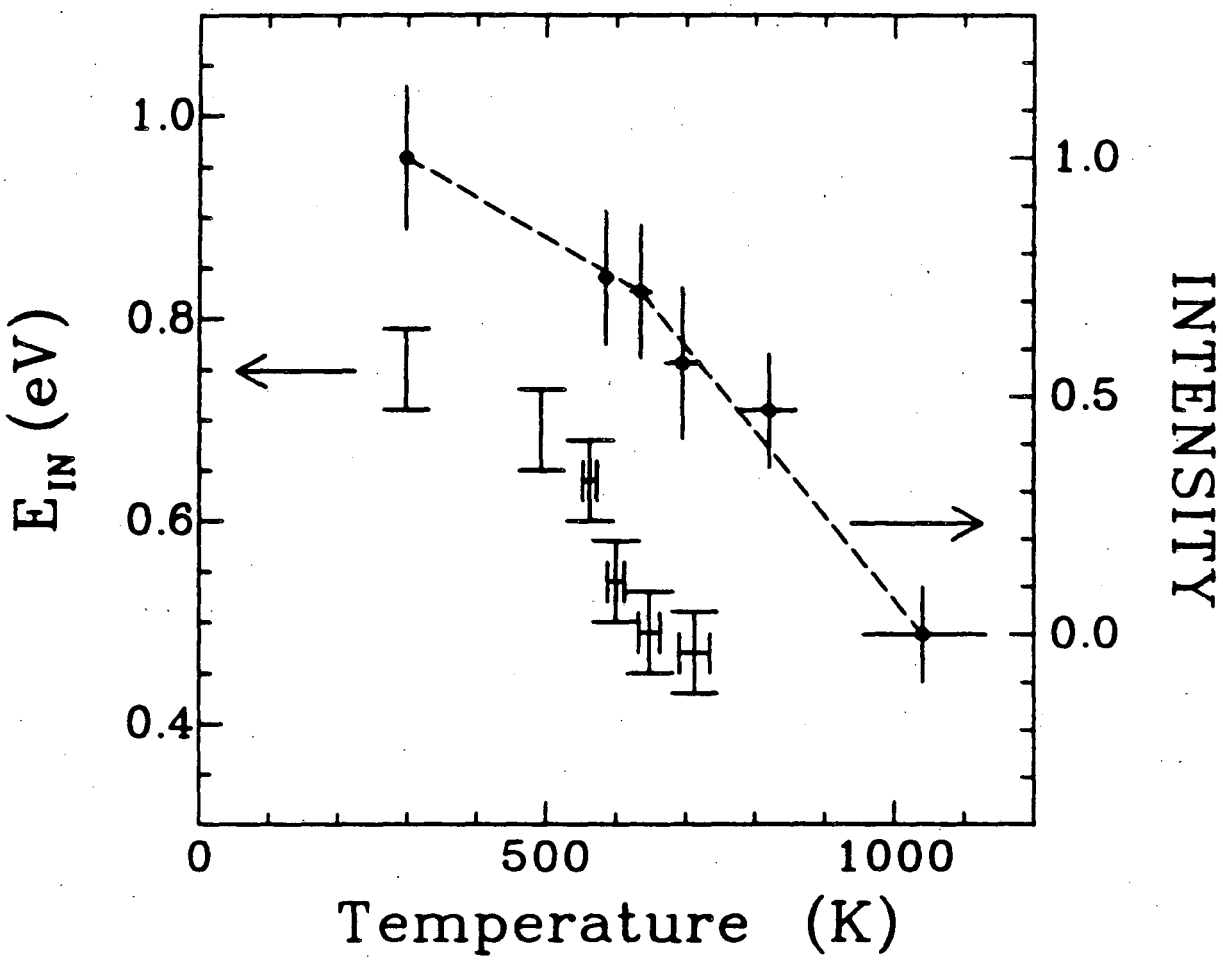

XBL 8412-5103

Figure 18

This report was done with support from the Department of Energy. Any conclusions or opinions expressed in this report represent solely those of the author(s) and not necessarily those of The Regents of the University of California, the Lawrence Berkeley Laboratory or the Department of Energy.

Reference to a company or product name does not imply approval or recommendation of the product by the University of California or the U.S. Department of Energy to the exclusion of others that may be suitable.

TECHNICAL INFORMATION DEPARTMENT
LAWRENCE BERKELEY LABORATORY
UNIVERSITY OF CALIFORNIA
BERKELEY, CALIFORNIA 94720